JOURNAL OF NEUROTRAUMA 37:2244–2260 (November 1, 2020)

DOI: 10.1089/neu.2020.7066

Red-Light (670 nm) Therapy Reduces Mechanical Sensitivity and Neuronal Cell Death, and Alters Glial Responses after Spinal Cord Injury in Rats

Di Hu,[1] Gila Moalem-Taylor,[2] and Jason R. Potas[1,2]

Abstract

Individuals with spinal cord injury (SCI) often develop debilitating neuropathic pain, which may be driven by neuronal damage and neuroinflammation. We have previously demonstrated that treatment using 670 nm (red) light irradiation alters microglia/macrophage responses and alleviates mechanical hypersensitivity at 7 days post-injury (dpi). Here, we investigated the effect of red light on the development of mechanical hypersensitivity, neuronal markers, and glial response in the subacute stage (days 1–7) following SCI.

Wistar rats were subjected to a mild hemi-contusion SCI at vertebra T10 or to sham surgery followed by daily red-light treatment (30 min/day; 670 nm LED; 35 mW/cm^2) or sham treatment. Mechanical sensitivity of the rat dorsum was assessed from 1 dpi and repeated every second day. Spinal cords were collected at 1, 3, 5, and 7 dpi for analysis of myelination, neurofilament protein NF200 expression, neuronal cell death, reactive astrocytes (glial fibrillary acidic protein [GFAP]$^+$ cells), interleukin 1 β (IL-1β) expression, and inducible nitric oxide synthase (iNOS) production in IBA1$^+$ microglia/macrophages. Red-light treatment significantly reduced the cumulative mechanical sensitivity and the hypersensitivity incidence following SCI. This effect was accompanied by significantly reduced neuronal cell death, reduced astrocyte activation, and reduced iNOS expression in IBA1$^+$ cells at the level of the injury. However, myelin and NF200 immunoreactivity and IL-1β expression in GFAP$^+$ and IBA1$^+$ cells were not altered by red-light treatment. Thus, red-light therapy may represent a useful non-pharmacological approach for treating pain during the subacute period after SCI by decreasing neuronal loss and modulating the inflammatory glial response.

Keywords: neuroinflammation; neuronal death; neuropathic pain; photobiomodulation; spinal cord injury

Introduction

The World Health Organization estimates between 250,000 and 500,000 people suffer from spinal cord injury (SCI) each year globally with an incidence of up to 1000 per million.[1,2] About 65–80% of patients with SCI develop neuropathic pain,[3–6] which is considered severe in 20–30% of cases.[7] Multitherapeutic approaches utilizing combinations of pharmacological intervention, exercise, massage, and physiotherapy are often employed to manage neuropathic pain; however, these approaches require significant resources from different professionals and family members, and are generally inefficient.[7,8]

Neuropathic symptoms, including sensory hypersensitivity (e.g., stimulus-evoked pain, dysesthesia, or pinprick hyperalgesia) in dermatomes corresponding to the lesion level are common is patients with SCI.[9] Numerous mechanisms have been implicated in the development of neuropathic pain following SCI, including structural damage (e.g., apoptosis, demyelination, and cytoskeletal damage), biochemical damage and excitotoxicity, neuroinflammation (e.g., glial activation and cytokine secretion), enzyme dysregulation, and neuronal hyperexcitability.[10] Microglia/macrophages, astrocytes, and oligodendrocytes can significantly influence neuropathic pain post-SCI.[11] For example, a major pro-inflammatory cytokine secreted by glial cells, interleukin 1 beta (IL-1β), is believed to sensitize dorsal horn neurons that are responsible for both the development of, and for providing positive feedback to enhance and maintain neuropathic pain.[12–16] Nitric oxide (NO), which is mainly derived from microglial inducible NO synthase (iNOS), has been shown to modulate long-term potentiation of C-fibers that eventually leads to hypersensitivity.[17] Several studies have shown that by altering some of these key inflammatory mediators, it might be possible to stall the development of neuropathic pain, or even depress its severity following SCI.[18–21]

[1]John Curtin School of Medical Research, Australian National University, Acton, Australian Capital Territory, Australia.
[2]Translational Neuroscience Facility, School of Medical Sciences, University of New South Wales, Sydney, Kensington, New South Wales, Australia.

Light therapy refers to the application of light irradiation, using laser or light-emitting diodes (LED), to modulate the cellular biology in the pursuit of clinical benefits. Wavelengths between 630 nm and 830 nm have been demonstrated to reduce glial activation and reduce secretion of inflammatory cytokines in different injury models, including SCI.[22,23] We have previously established that 670 nm treatment in SCI rats reduces microglia/macrophage activation and alleviates mechanical hypersensitivity at 7 days post-injury (dpi).[21] In the present study, we examined the effects of 670 nm treatment during the subacute phase of recovery (prior to 7 dpi) following SCI on: 1) the development of mechanical hypersensitivity; 2) myelination and neuronal apoptosis; and 3) astrocyte and microglia/macrophages presence in the spinal cord and their associated IL-1β and/or iNOS expression in the white matter tracts.

Methods

Animals and spinal cord injury

Sibling male Wistar rats, 52 ± 4 days old, were used for this study with ethics approvals from the Australian National University Animal Experimentation Ethics Committee. Animals were held in individually ventilated cages with environmental enrichment, standard food, and water *ad libitum.* The housing facility was maintained at 20°C with a 12-h dark/light cycle. Animals were housed for 2 weeks prior to experimentation, and all experiments were carried out during the light cycle. Animals were anesthetized using isoflurane (1.7–2.3 v/v %) while being maintained at 37°C by a heat mat during all surgical procedures. Laminectomy was performed at the T10 vertebra, where the dura mater and arachnoid were removed. A 10-g weight drop from 25 mm above the spinal cord was used to induce a hemi-contusion on the right side of the spinal cord.[21,24] Sham-injured animals underwent the same surgical procedures without the impaction. All animals received subcutaneous injections of antibiotics (cephalothin sodium; DBL) after surgery and once every 24 h throughout the recovery period at a dosage of 15 mg/kg/12 h. Animals were returned to their home cage after the effects of anesthesia had subsided.

Treatment

SCI animals were divided into untreated (SCI; $n = 40$) and 670 nm treated (SCI+670; $n = 33$) groups. Sham-injured animals were divided into untreated (sSCI; $n = 12$) and 670 nm treated sSCI+670; $n = 11$ groups. Treatments commenced 2 h after the surgery and were repeated every 24 h after behavioral sensitivity testing. For the duration of the treatment, animals were contained in a transparent Perspex box in their own cages. A commercially available LED array (75 mm^2) that provided light at 670 ± 15 nm with a measured irradiance of 35.4 ± 0.05 mW/cm^2 (WARP 75A; Quantum Devices, Inc.) was placed directly above a Perspex box for light-treated animals (SCI+670 and sSCI+670 groups). With this light source, we have previously measured the irradiance at the ventral surface of the spinal cord to be 3.2 ± 0.6 mW/cm^2 in a similar cohort of animals, as well as have described details of the spectral features and irradiance measurements of this light source.[21] The treatments were delivered for 30 min per day (63.7 ± 0.09 J/cm^2 per session) to the dorsal surface of the animal. Untreated animals (SCI and sSCI groups) were handled in the same way without the LED being turned on (sham treatment).

Sensitivity testing

All animals were subjected to sensitivity testing on every odd day from 1 dpi as we have previously described.[21] All sessions were carried out by the same assessor, who was blinded to experimental groups. Briefly, a nylon filament (OD: 1.22 mm; mass delivered: 2.86 ± 0.09 g) was used to deliver non-noxious tactile stimuli to six defined regions: dermatomes innervated by nerves above the level of the injury (dermatomes C6–T3), at the level of the injury (dermatomes T9–12), and below the level of the injury (dermatomes L2–5) on both ipsilateral and contralateral sides. At each region, 10 consecutive stimuli were applied, and responses were categorized into four different categories: 1) no response; 2) acknowledgement of the stimulus; 3) sign of pain avoidance behavior including moving away from the stimulus; 4) severe pain avoidance behavior including jumping, running, and vocalization. The categories were then assigned a weight individually (0, 1, $\sqrt{2}$, and 2) and the summation of the 10 responses gave the regional sensitivity score (RSS). The summation of the six RSSs gave the cumulative sensitivity score (CSS). A group of age-matched male Wistar rats were also included in the sensitivity testing as non-injured control animals (CON; $n = 7$). A hypersensitivity threshold was defined as 2 standard deviations (SDs) above the mean of CON animals. Hypersensitivity incidence was thus calculated as the percentage of animals whose CSS exceeded the hypersensitivity threshold. See the article by Hu and colleagues for more details on sensitivity testing.[21]

Tissue collection and processing

At the end of designated recovery periods (1, 3, 5, and 7 dpi), animals were euthanized and perfused transcardially with 0.9% (w/v) saline followed by 4% (w/v) paraformaldehyde. The spinal cord was dissected, and then it was cryoprotected in 30% (w/v) sucrose solution for at least 24 h before cryosectioning. Spinal cord sections 1.5 mm rostral and 1.5 mm caudal to the injury epicenter were placed in Tissue-Tek optimal cutting temperature (OCT) compound (IA018; Proscitech) and then sectioned horizontally at 20 μm thickness on a cryostat (CM1850; Leica Microsystems) at −20°C.

Terminal deoxynucleotidyl transferase dUTP nick end labeling

The same protocol was used as published previously.[21] Slides were incubated with 1:10 terminal deoxynucleotidyl transferase (TdT) buffer for 10 min and subsequently in reaction mixture (0.12% v/v TdT [3333574001, Roche Applied Science]; 0.25% v/v 2'-deoxyuridine 5'-triphosphate [dUTP; 11093070910, Roche Applied Science]; 10.51% v/v TdT buffer) for 1 h at 37°C. This was followed by 15 min incubation with 1:10 saline-sodium citrate (SSC) buffer and blocking with 10% v/v normal goat serum in 0.1 M phosphate-buffered saline (PBS) for 10 min. Slides were then incubated with 0.1% v/v streptavidin 488 (S-11223, Invitrogen) at 37°C for 30 min. This was followed by immunohistochemistry where appropriate.

Immunohistochemistry

Standard immunohistochemistry procedures were followed. Slices around the injury epicenter were dehydrated in 70% ethanol and then rehydrated in distilled water and subsequently in 0.1 M PBS. The antigen retrieval step involved incubation in Reveal-it Solution (AR2002, ImmunoSolution) for 6–12 h at 37°C followed by 0.1 M PBS washes. Slides were blocked in 20% (v/v) normal donkey serum in 0.1 M PBS with 0.1% (w/v) bovine serum albumin (BSA) for 1 h at room temperature before the addition of primary antibodies. Primary antibodies (myelin basic protein [1:1000, Abcam ab40390], NeuN [1:200, Abcam ab104224], NF200 [1:1000, Invitrogen 131200], glial fibrillary acidic proteim [GFAP; 1:1000, Dako Z0334], IL-1β [1:200, R&D systems AF501-NA], IBA1 [1:200, Wako 019-19741 and Abcam ab5076], and uNOS [1:150, Invitrogen PA1-039]) were diluted in 0.1M PBS containing 2%

(v/v) normal donkey serum and 0.1% (w/v) BSA and then were incubated overnight at 4°C. Negative controls were also included where the primary antibodies were excluded.

Slides were washed with 0.1M PBS followed by secondary antibody incubations at room temperature for 1–2 h. Secondary antibodies (goat anti mouse Alexa Fluor 488 [1:1000, Invitrogen A-11001], goat anti rabbit Alexa Fluor 594 [1:1000, Invitrogen A-31631], donkey anti-goat Alexa Fluor 594 [1:500, Abcam ab150132], and donkey anti-rabbit Alexa Fluor 488 [1:1000, Invitrogen A-21206]) were diluted in the same way as primary antibodies and followed by 0.1 M PBS washes. Slides were then incubated in 1:1000 (v/v) diluted Hoechst solution (94403; Sigma-Aldrich) and then washed off using 0.1 M PBS.

Image acquisition and quantification

Slides were scanned and imaged using a Nikon A1 confocal microscope fitted with a camera (DS-Qi1; Nikon). In MBP/NF200/Hoechst staining, the entire cross section of the spinal cord at the injury epicenter was scanned using three lasers (405 nm, 488 nm, and 561 nm) under 10× magnification with a z-plane of at least 10 μm in depth. In NeuN/TUNEL/Hoechst staining, six representative images were imaged in the dorsal, intermediate, and ventral regions of the spinal cord on both ipsilateral and contralateral sides under 20× magnification using the same lasers and the same z-plane configurations as above. All imaging and laser settings were kept constant for all animals for each staining. Images were then transferred offline for analysis using ImageJ version 1.46r.[25] NeuN/Hoechst and NeuN/TUNEL/Hoechst stainings were analyzed using the Cell Counter plugin as described earlier.[21] NF200 was expressed as particles (density/mm^2). The regions of interest were defined and quantified prior to cell counting covering a minimum area of 0.1 mm^2. Myelin basic protein (MBP) was analyzed as % area of fluorescence.

In GFAP/Hoechst staining, the entire cross section of the spinal cord at the injury level was scanned using two lasers (405 nm and 488 nm) under 10× magnification with a z-plane of at least 10 μm in depth. In GFAP/IL1β/Hoechst, IBA1/IL-1β/Hoechst, and IBA1/uNOS/Hoechst staining, six representative images were taken in the dorsal, lateral, and ventral spinal cord funiculi at the injury level on both ipsilateral and contralateral sides under 20× magnification using three lasers (405 nm, 488 nm, and 561 nm) and the same z-plane configuration as above. All imaging and laser settings were kept constant for all animals for each staining. Images were then analyzed offline using ImageJ version 1.46r.[25] GFAP was analyzed as fluorescence per % area, whereas GFAP/IL-1β/Hoechst, IBA1/IL-1β/Hoechst, and IBA1/uNOS/Hoechst stainings were analyzed using the Cell Counter plugin as described earlier.[21] The areas of interest were defined and quantified prior to cell counting covering a minimum area of 0.1mm^2. Cell quantification is expressed as the number of cells per unit area (mm^2).

Statistical analysis

All data were expressed as mean ± standard error of the mean (SEM) unless otherwise stated. Statistical analysis was carried out using R.[26] General linear mixed-effects models (GLMER; *glmer* function in R for binomially distributed data) or linear mixed-effects models implementing Satterthwaite's approximation (LMER; *lmer* function in R) were used for multiple factor analysis accounting for random effects.[27] LMER was followed by Tukey or false discover rate post hoc adjustments for pairwise comparisons implemented by estimated marginal means (*emmeans* fuction in R) where appropriate. Log transformations (log[x + 1]) were performed when the data were heteroscedastic and improved model fitting. Model fitting was assessed by inspection of residual plots and calculating Akaike information criterion (*AIC* function in R).[28]

For data that failed to fit LMER models, a cumulative link mixed model was fitted, accommodating one random factor, with the Laplace approximation (CLMM; *clmm2* function in R).[29] The CLMM required categorizing scores into bins that best represented the data. Histograms of complete data sets (blind to groups) were inspected to determine natural breaks in the data to define each category. CLMM models were assessed with Akaike information criterion as well as inspection by plotting the observed data against the model predicated values, and comparing a linear model made with these data to a line with an intercept of zero and a slope of 1. Post hoc pairwise comparisons were performed using a Wilcoxon rank sum test on raw scores where applicable, with Bonferroni *p*-value correction.

Both models accommodated up to four fixed factors (treatment, side, regions, and time) and one (CLMM: animal identification) or two (LMER: animal identification nested within their respective families) random factors. Models of CSSs were confirmed against models of RSSs, which enables more factors and thereby improved model fitting and statistical power. *P*-values less than 0.05 were considered as statistically significant.

Results

Red-light reduces the level and incidence of mechanical hypersensitivity

To determine whether red-light treatment affects mechanical hypersensitivity during the subacute phase of SCI, we measured mechanical sensitivity in control, untreated, and light-treated SCI and sham-operated rats. We first assessed the range of CSSs of uninjured CON animals by quantifying the sum of RSSs of uninjured normal CON animals ($n = 7$; Fig. 1A). Most animals had a mix of category 1 and category 2 responses, except for one animal that demonstrated two category 3 responses at the contralateral Above-Level region. The CON group had a mean CSS of 2.75 and a SD of 2.09, and consequently a hypersensitivity threshold of 6.92 (mean +2× SD) was established. The Above-Level region was more sensitive than the At-Level region ($p = 0.041$, LMER, Tukey post hoc), whereas differences between sides failed to reach significance ($p = 0.073$, LMER).

We then quantified mechanical sensitivity responses at 1–7 dpi in animals with SCI (SCI, untreated) and SCI with 670 nm light treatment (SCI+670, Fig. 1B; see Fig. 2 for *n* values). Compared with the CON group, CSSs were significantly elevated in the SCI group ($p = 0.040$, LMER, Tukey), but not the SCI+670 group ($p = 0.55$, LMER, Tukey) over the 7-day recovery period. Further, the SCI+670 group displayed a significant reduction of CSSs compared with the SCI group ($p = 0.0097$, LMER, Tukey). There was no time effect ($p = 0.86$) or interaction between treatment and time ($p = 0.80$) in the SCI groups (Fig. 1B).

In sham-injured groups (sham-injured + untreated, sSCI; sham-injured + 670 nm treated, sSCI+670) that were subjected to the same sensitivity testing (Fig. 1C), a significant effect of red-light treatment on CSSs was observed ($p = 0.018$, CLMM). Post hoc analysis revealed that CCSs of sSCI animals were not significantly different from those of the CON group ($p = 1.0$, Wilcoxon rank sum, Bonferroni adjusted); however, interestingly, the CSSs of the sSCI+670 group was significantly reduced compared with both CON and sSCI groups ($p = 0.0003$ and $p = 0.0075$, respectively; Wilcoxon rank sum, Bonferroni adjusted).

To assess the spatial effects of injury and treatment on mechanical hypersensitivity, RSSs in six regions were analyzed across up to 7 dpi (Fig. 2, Supplementary Figs. S1 and S2). Congruent with the analysis above, the SCI+670 group displayed an overall

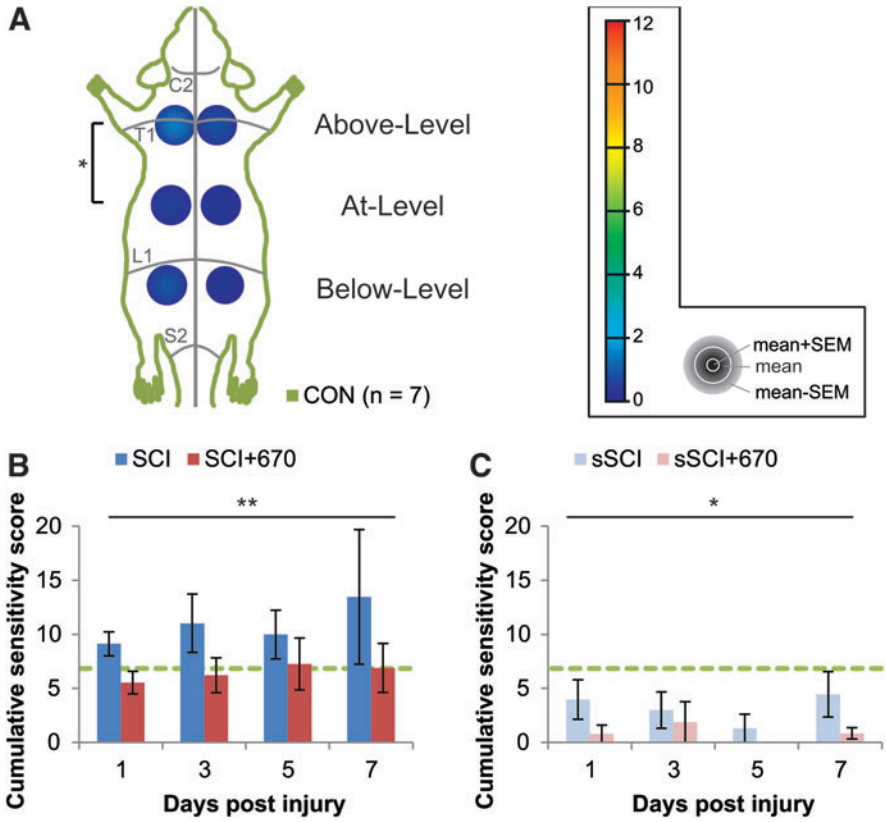

FIG. 1. Cumulative sensitivity is increased up to 7 dpi following mild T10 hemi-contusion SCI but reduced after red-light treatment. **(A)** RSSs of the CON group ($n = 7$) showing the mean + SEM, mean, and mean – SEM in concentric order as indicated by the color scale and accompanying gray legend (insert). RSSs, obtained from six regions (left and right sides; ''Above-Level,'' ''At-Level,'' and ''Below-Level'' relative to T10 injury), are overlaying a schematic representation of the rat dorsum, with C2, T1, L1, and S1 dermatomes and midline indicated (gray lines). Statistical comparison between levels is indicated by the black bracket. **(B)** CSSs in all spinal-cord injured animals with (SCI+670) or without (SCI) red-light treatment. **(C)** CSSs in all sham-injured animals with sSCI+670 or without (sSCI) red-light treatment. Green-dashed line indicates hypersensitivity threshold (6.92) derived from CON group (see Methods section). Statistical comparison between levels in CON group (vertical bracket, CLMM) and between SCI and SCI+670 groups across the time-points (black line, CLMM) are indicated. Data are expressed as mean ± SEM; $*p < 0.05$, $**p < 0.01$. See Figure 2 for n values for all groups at each time-point. CLMM, cumulative link mixed model; CSS, cumulative sensitivity score (sum of RSSs); CON, non-injured control; dpi, days post-injury; RSS, regional sensitivity score; SEM, standard error of the mean. Color image is available online.

reduction in mechanical sensitivity compared with the SCI group ($p = 0.004$, CLMM; Fig. 2A–D, left panel), and similarly, the sSCI+670 group also displayed a significant reduction in mechanical sensitivity compared with the sSCI group ($p = 0.006$; CLMM; Fig. 2A–D, right panel). For injured groups, the treatment effect was most evident at 1 dpi ($p = 0.010$, Fig. 2A, left) and 3 dpi ($p = 0.024$, Fig. 2B, left), whereas for the sham-injured groups, the effect of red-light was most obvious at 1 dpi ($p = 0.029$, Fig. 2A, right). Interestingly, a significant reduction of RSSs following red-light treatment in both injured and sham-injured groups was detected in animals that did not develop hypersensitivity (Supplementary Fig. S1).

To determine whether red-light treatment also affects the incidence of animals developing mechanical hypersensitivity (see Supplementary Fig. S2 for RSSs), we analyzed the proportion of animals with a CSS greater than the hypersensitivity threshold in all treatment groups from day 1–7 following SCI or sham injury (Table 1). Following injury, over half of the SCI group developed hypersensitivity up to 5 dpi, and only approximately one-third in the SCI+670 group. Although the effect of red-light significantly reduced the incidence of developing hypersensitivity over the 1- to 5-dpi period ($p = 0.037$, GLMER), the effect failed to reach significance across the entire 7-day period ($p = 0.080$, GLMER). There was no significant difference in the incidence of sham-injured animals reaching the hypersensitivity threshold between the two groups; however, only a few animals in each group developed hypersensitivity (Table 1).

These behavioral results indicate that red-light treatment reduces mechanical sensitivity scores following both SCI and sham injury, and that red-light treatment reduces the incidence of developing hypersensitivity for at least the first 5 days.

Red-light does not affect the level of myelination and heavy neurofilament expression

To determine whether red-light treatment affects axons in the injured spinal cord, immunohistochemical analysis was carried out to assess the degree of myelination (MBP staining) and density of axons (NF200 expression) at different time-points post-injury.

The percentage area of positive MBP staining was analyzed from both sides over the recovery points in both SCI groups (Fig. 3). On the side contralateral to the injury (Fig. 3C), the

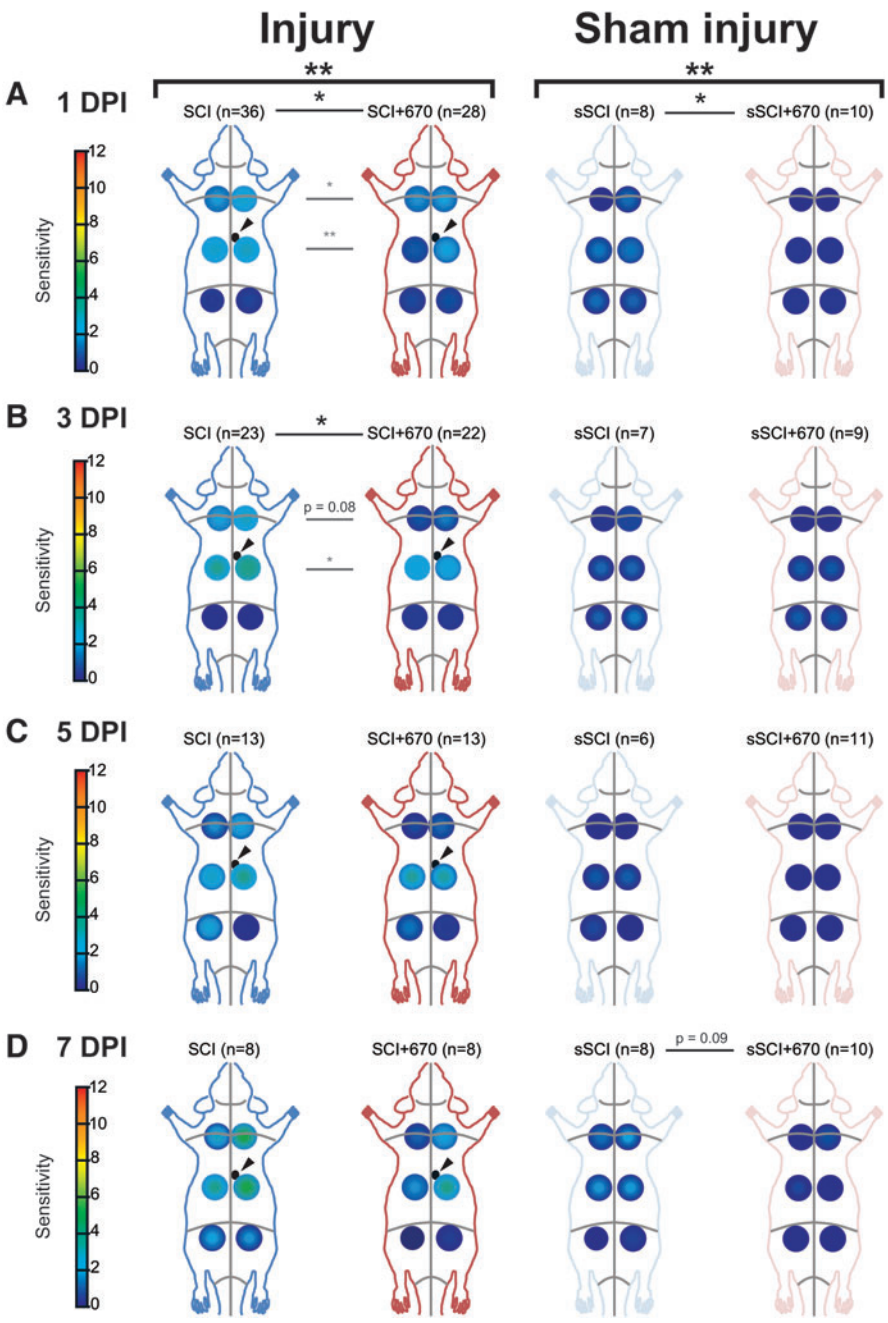

FIG. 2. At-Level and Above-Level regional sensitivity are reduced by red-light treatment. RSSs in SCI (blue), SCI+670 (red), sSCI (light blue), and sSCI+670 (pink) animals at **(A)** 1 dpi, **(B)** 3 dpi, **(C)** 5 dpi, and **(D)** 7 dpi are shown for all animals investigated. Arrowheads indicate location of T10 hemi-contusion injury (small black circles) in SCI groups. Statistical comparisons between two groups across all time-points (black bracket, CLMM), across all levels at individual time-points (black lines, CLMM), and between two groups at different levels (gray lines, CLMM) are indicated. Data are expressed as mean ± SEM as per Figure 1A inset; *n* values indicated for each group; *$p < 0.05$, **$p < 0.01$, *p*-value indicated for $0.1 < p < 0.05$. CLMM, cumulative link mixed model; dpi, days post-injury; RSS, regional sensitivity score; SCI, spinal-cord injured untreated; SCI+670, spinal-cord injured + red-light treatment; sSCI, sham-injured untreated; sSCI+670, sham-injured + red-light treatment; SEM, standard error of the mean. Color image is available online.

percentage area positive for MBP staining was around 50–60% throughout the recovery period in both groups. This level of staining was similar to the CON group (Fig. 3C). On the ipsilateral side of the spinal cord (Fig. 3D), there was significantly less area of MBP^+ staining compared with the contralateral side in both injury groups ($p = 1.5e\text{-}08$, LMER). Compared with the CON group, the ipsilateral side was significantly reduced in both the SCI ($p = 0.004$, LMER) and SCI+670 ($p = 0.0362$, LMER) groups.

Analysis of the heavy neurofilament NF200 in the spinal cord gray matter following injury with and without 670 nm treatment (Fig. 4) was carried out from three regions (dorsal, intermediate, and ventral) across both sides of the spinal cord (Fig. 4A). In CON

Table 1. Red-Light Treatment Reduces Hypersensitivity Incidence after a Mild T10 Hemi-Contusion SCI

Days post-injury	*SCI (% hypersensitive)*	*SCI+670 (% hypersensitive)*	*sSCI (% hypersensitive)*	*sSCI+670 (% hypersensitive)*
1 dpi	56% ($n=20$)	32% ($n=9$)	25% ($n=2$)	10% ($n=1$)
3 dpi	57% ($n=13$)	31% ($n=7$)	14% ($n=1$)	11% ($n=1$)
5 dpi	54% ($n=7$)	23% ($n=3$)	17% ($n=1$)	0
7 dpi	38% ($n=3$)	50% ($n=4$)	25% ($n=2$)	0

Hypersensitivity incidence following SCI or sham-SCI is shown for untreated and red-light-treated groups, as the percentage of animals with scores above the hypersensitivity threshold (see Fig. 1 for threshold, see Supplementary Fig. S2 for RSSs of hypersensitive animals).
dpi, days post-injury; RSS, regional sensitivity score; SCI, spinal cord injury.

animals, all six regions showed comparable levels of NF200 density (a total average of 12,575 ± 915 particles/mm^2) with no significant difference on either side ($p=0.94$, LMER), region ($p=0.50$, LMER), or combinations of side and region ($p=0.97$, LMER; Fig. 4C–H).

Following SCI, there was an overall significant reduction in NF200 density across all regions and sides of the spinal cord compared with the control group (SCI, $p=0.0002$; SCI+670, $p=0.0004$; LMER, Tukey). No significant differences between the SCI and SCI+670 groups across all regions and sides was observed ($p=0.71$, LMER). The dorsal regions showed a significant reduction compared with the intermediate ($p=0.031$, LMER, Tukey) and ventral ($p=0.0002$, LMER, Tukey) regions. Across all regions and sides, the 7 dpi time-point showed an overall significant reduction in NF200 density compared with earlier time-points (1–3 dpi; $p \leq 0.037$, LMER, Tukey). This time effect arose from the intermediate ($p=0.0012$; LMER, Tukey) and ventral ($p=5.6e-6$, LMER, Tukey) regions (Fig. 4E–H), but not the dorsal region ($p=0.79$, LMER, Tukey, Fig. 4C,D), which displayed a significant reduction of NF200 particle density on the ipsilateral side ($p=0.014$, LMER, Tukey).

Red-light ameliorates the level of neuronal cell death

We stained the spinal cords against NeuN/DAPI (Supplementary Fig. S3), as well as NeuN/TUNEL/DAPI, which marks neuronal cells undergoing apoptosis or necrosis (Fig. 5). There was no significant difference between groups in NeuN cell density, despite a strong reduction in the ipsilateral side across all levels ($p<2e-16$, LMER; Supplementary Fig. S3). Analysis of neuronal cell death was carried out on the six regions of interest across both sides of the spinal cord gray matter (Fig. 5A). Examples of NeuN/TUNEL/DAPI staining in both SCI and SCI+670 groups are shown in Figure 5B. The vast majority of triple-labeled cells

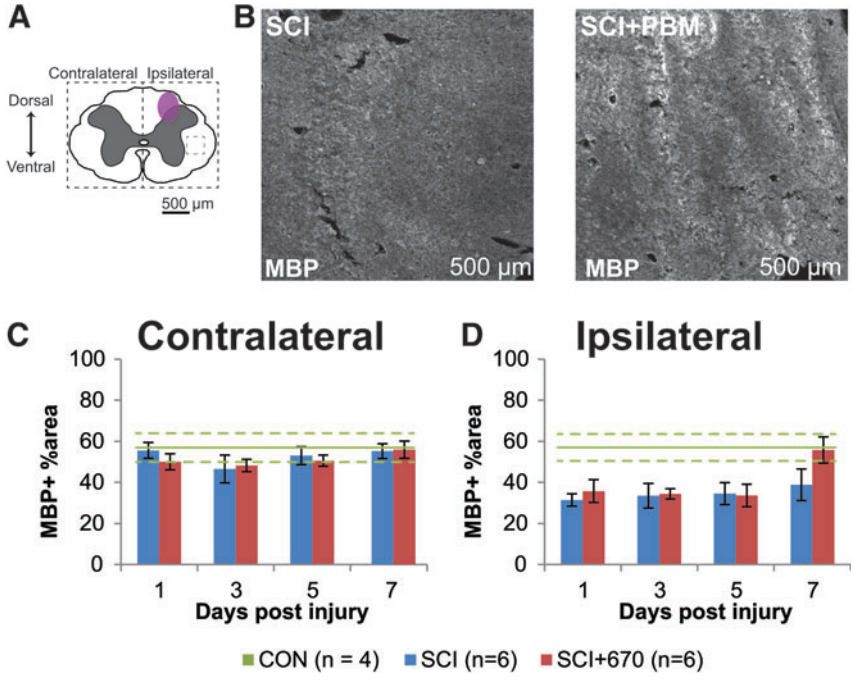

FIG. 3. Ipsilateral demyelination was observed from 1–5 dpi post hemi-contusion SCI. **(A)** Schematic representation of the spinal cord illustrates the approximate location of the injury epicenter (purple shaded area) and region of interest (dotted) for MBP labeling quantification. **(B)** Example images are shown of positive MBP labeling (white) from sham- and light-treated groups ipsilateral to the injury at the dorsal level at 7 dpi (region of example images indicated by small dashed box in A). **(C,D)** Quantification of MBP-positive labeling, expressed as the percentage area of positive label above background within the region of interest (dotted boundaries in A), contralateral (C), and ipsilateral (D) to the injury of sham- and light-treated groups. Data for control animals are shown (solid green, mean; dotted green, SEM. All other data expressed as mean ± SEM; *n* values indicated (legend) are for each time-point. dpi, days post-injury; MBP, myelin basic protein; SCI, spinal cord injury; SEM, standard error of the mean. Color image is available online.

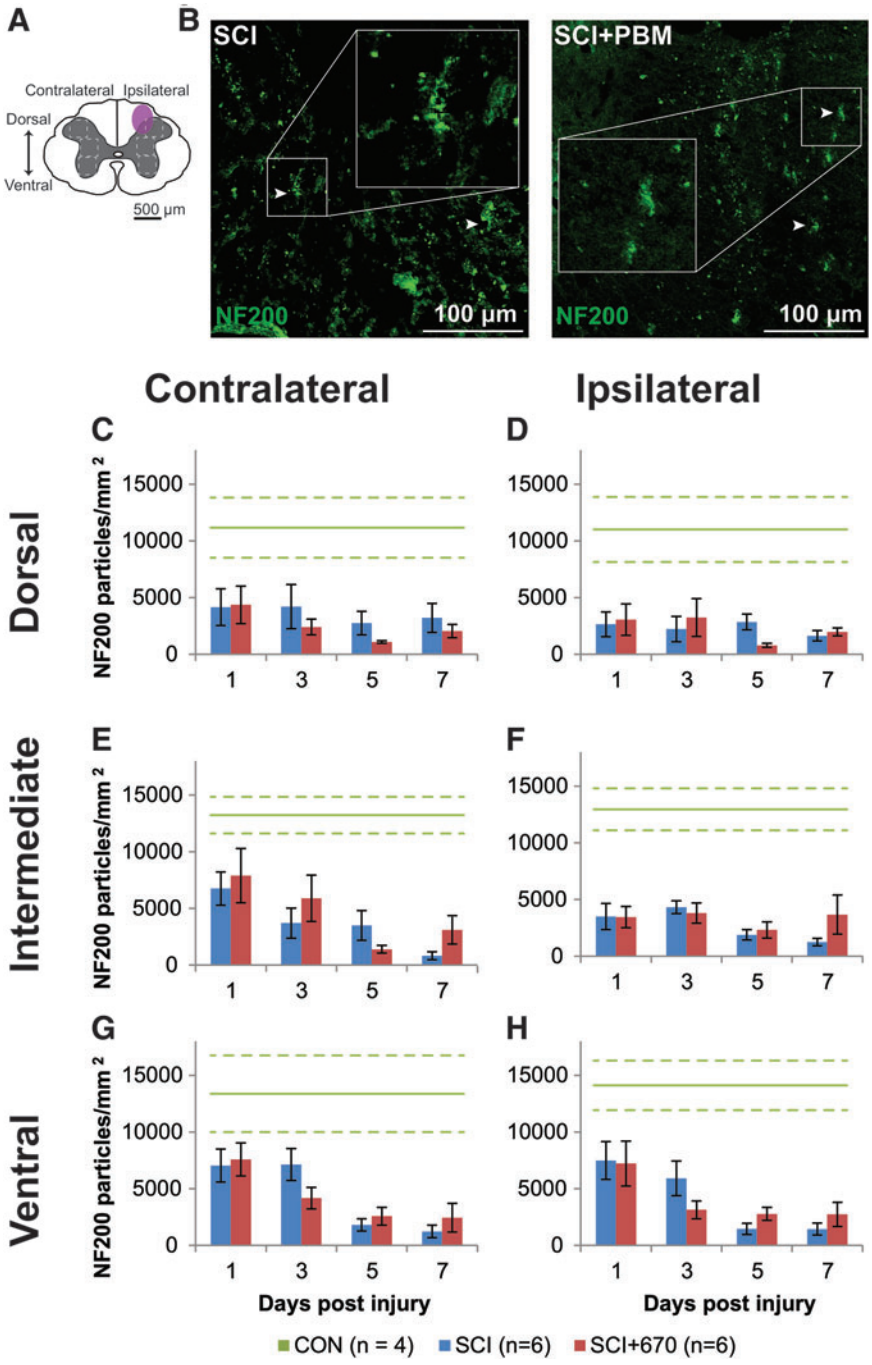

FIG.4. NF200 density is reduced following spinal cord injury but not altered by red-light treatment. **(A)** The schematic representation of the spinal cord illustrates the dorsal, intermediate, and ventral regions of interest for analysis (enclosed by dashed lines, 0.1 mm^2). Approximate location of injury is indicated (purple shaded area). **(B)** Example images of NF200 (green) positive labeling from spinal-cord injured sham- and light-treated groups ipsilateral to the injury at dorsal level at 7 dpi. **(C,D)** Quantification of $NF200^+$ labeling expressed as positive particle density within the region of interest, in the dorsal region of the spinal cord, contralateral (C) and ipsilateral (D) to the injury of sham- and light-treated groups. **(E,F)** $NF200^+$ particle density in the intermediate regions of interest contralateral (E) and ipsilateral (F) to the injury. **(G,H)** $NF200^+$ particle density in the ventral regions of interest contralateral (G) and ipsilateral (H) to the injury. Data for control animals are shown (solid green, mean; dotted green, SEM). All other data expressed as mean ± SEM; *n* values indicated for each time-point (legend). See text for statistical comparisons. dpi, days post-injury; SCI, spinal-cord injured animals without red-light treatment; SCI+670, spinal-cord injured animals with red-light treatment; SEM, standard error of the mean. Color image is available online.

arose at 1 dpi across all sides and regions (Fig. 5C–H). At this time-point, red-light treatment significantly reduced the density of $NeuN^+TUNEL^+DAPI^+$ cells across all regions from the ipsilateral ($p = 0.0009$, LMER) but not contralateral side ($p = 0.28$, LMER).

Red-light reduces astrocyte reactivity in the spinal cord

We have previously demonstrated reductions in activated microglia/macrophages following 670 nm treatment in SCI rats after 7 days of recovery.[21] To examine whether red-light treatment

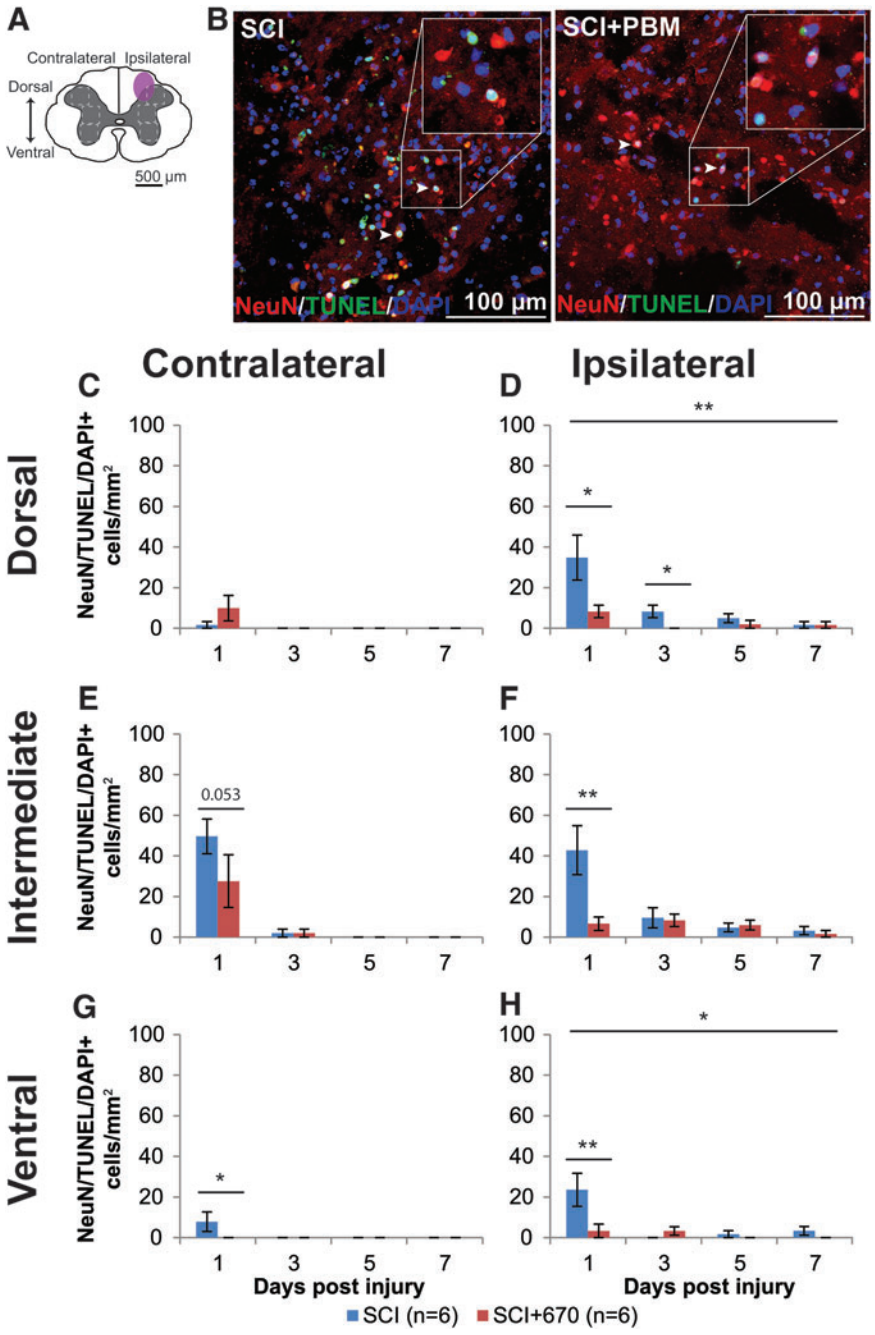

FIG. 5. Neuronal cell death occurs early following spinal cord injury, which is reduced by 670 nm treatment. **(A)** The schematic representation of the spinal cord illustrates the dorsal, intermediate, and ventral regions of interest for analysis (enclosed by dashed lines, 0.1 mm^2). Approximate location of injury epicenter is indicated by the purple shaded area. **(B)** Example images of NeuN (red), TUNEL (green), and DAPI (blue) triple-positive cells from SCI untreated and light-treated groups ipsilateral to the injury at dorsal region at 1 dpi. **(C,D)** Quantification of $NeuN^+TUNEL^+DAPI^+$ cells, expressed as triple-positive cell density within the region of interest, in the dorsal region of the spinal cord, contralateral (C) and ipsilateral (D) to the injury of untreated and light-treated groups. **(E,F)** $NeuN^+TUNEL^+DAPI^+$ cell density in the intermediate regions of interest contralateral (E) and ipsilateral (F) to the injury. **(G,H)** $NeuN^+TUNEL^+DAPI^+$ cell density in the ventral regions of interest contralateral (G) and ipsilateral (H) to the injury. Data are expressed as mean ± SEM; *n* values indicated (legend) are for each time-point. Statistical comparisons between SCI and SCI+670 (LMER) are shown; $*p < 0.05$, $**p < 0.01$. dpi, days post-injury; LMER, linear mixed-effects models; SCI, spinal-cord injured animals without red-light treatment; SCI+670, spinal-cord injured animals with red-light treatment; SEM, standard error of the mean. Color image is available online.

also influences astrogliosis in the injured spinal cord, astrocyte activation was quantified as the percentage area of $GFAP^+$ immunofluorescence across six regions of the spinal cord (Fig. 6A). Examples of $GFAP^+$ staining for SCI and SCI+670 groups are shown in Figure 6B. Across groups, spinal cord regions and time, $GFAP^+$ area was significantly increased ipsilateral to the injury compared with the contralateral side ($p = 6.3e\text{-}14$, LMER). Across all spinal cord regions, sides, and time, red-light significantly reduced the $GFAP^+$ area ($p = 0.0081$, LMER), which mainly arose 3–7 dpi ($p = 0.0063$, LMER). A group difference was evident in

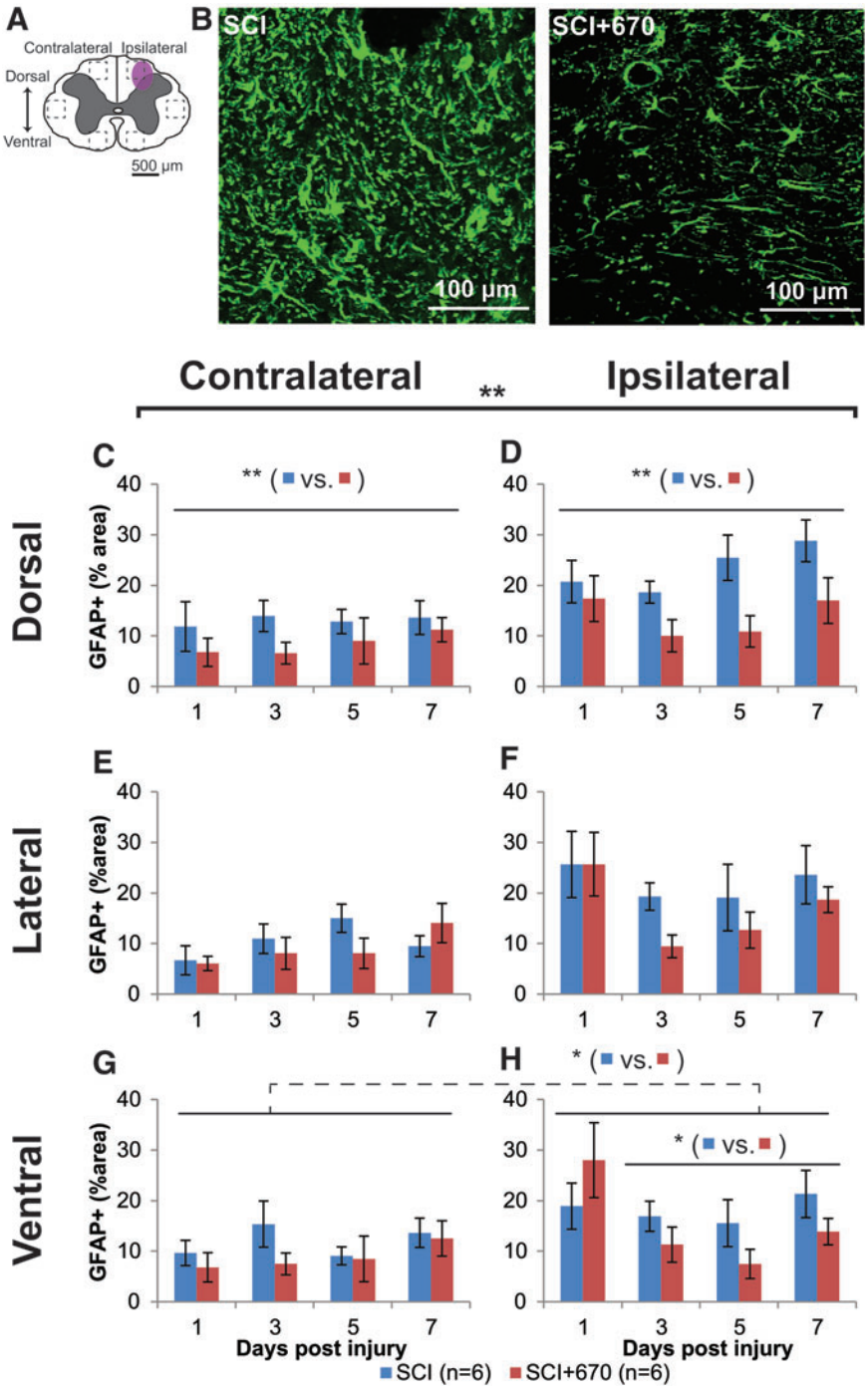

FIG. 6. Spinal-cord injury induced astrocyte activation is reduced following red-light treatment. **(A)** The schematic representation of the spinal cord illustrates the dorsal, lateral, and ventral regions of interest for analysis (enclosed by dashed lines, area of each box: 0.1 mm^2). Approximate location of injury is indicated by the purple shaded area. **(B)** Example images are shown of positive GFAP labeling (green) from untreated and light-treated groups ipsilateral to the injury at the dorsal region at 3 dpi. **(C,D)** Quantification of $GFAP^+$ labeling, expressed as the percentage area of positive label above threshold within the dorsal regions of interest contralateral (C) and ipsilateral (D) to the injury of untreated and light-treated groups. **(E,F)** $GFAP^+$ label in the lateral regions of interest contralateral (E) and ipsilateral (F) to the injury. **(G,H)** $GFAP^+$ label in the ventral regions of interest contralateral (G) and ipsilateral (H) to the injury. For each time-point *n* values are indicated (legend). Statistical comparisons between SCI and SCI+670 groups across all time-points and regions (black bracket) and across the time-points at different region (black line) are indicated. Dotted line indicates significance across both sides. Data are expressed as mean ± SEM; $*p < 0.05$, $**p < 0.01$ (LMER). GFAP, glial fibrillary acidic protein; LMER, linear mixed-effects models; SCI, spinal-cord injured animals without red-light treatment; SCI+670, spinal-cord injured animals with red-light treatment; SEM, standard error of the mean. Color image is available online.

the dorsal (Fig. 6C,D, $p=0.0027$, LMER) and ventral (Fig. 6G,H, $p=0.046$, LMER) regions of the spinal cord over the 3- to 7-day recovery period, but this failed to reach significance in the lateral region (Fig. 6E,F, $p=0.148$, LMER).

To determine if GFAP levels on the contralateral side at 1 dpi were elevated compared with CON animals, GFAP expression 24 h post-injury (SCI, $n=4$) and sham-injury (sSCI, $n=4$) were compared with normal animals (CON, $n=4$; Supplementary Fig. S4). Overall, 24 h after injury, the $GFAP^+$ area was elevated in the SCI group on both sides of the spinal cord compared with the CON group (contralateral, $p=0.001$, ipsilateral $p<0.001$, LMER, Tukey) and sSCI animals (contralateral, $p=0.007$, ipsilateral $p<0.001$, LMER, Tukey). Compared with the CON animals, the sSCI animals failed to reach significant difference on the contralateral side ($p=0.60$, LMER, Tukey), and was significantly increased but with a small effect size in the ipsilateral side ($p<0.049$. LMER, Tukey; Supplementary Fig. S4C).

These results demonstrate that astrocytes are already elevated across both sides of the spinal cord following hemi-contusion as early as 1 dpi at the spinal segment of injury, but more so on the ipsilateral side. GFAP expression is not affected by red-light at 1 dpi, but is significantly suppressed by 670 nm treatment from 3 dpi onward.

Red-light does not affect IL-1β expression in glial cells

IL-1β is a pro-inflammatory cytokine that plays a key role in pain signaling.[30] We therefore investigated IL-1β expression in astrocytes and microglia/macrophages in six regions across the spinal cord (Fig. 7A; Fig. 8A) following hemi-contusion and 670 nm treatment. Examples of IL-$1\beta^+GFAP^+$ cells, defined as triple positive for IL-1β, GFAP, and DAPI, are shown in Figure 7B, and of IBA1, IL-1β, and DAPI, are shown in Figure 8B.

Throughout the spinal cord (Fig. 7C-H), IL-$1\beta^+GFAP^+$ cell density was elevated on the ipsilateral side compared with the contralateral side ($p=2.7e-07$, LMER), whereas there was no overall significant effect of red-light treatment ($p=0.18$). At the dorsal region, a time effect was apparent ($p=0.046$, LMER), notably that the 5-dpi time-point was significantly elevated compared with the 1-dpi time-point across both sides ($p=0.030$, LMER, Tukey). This significant IL-$1\beta^+GFAP^+$ cell density elevation at the 5-dpi time-point in the dorsal region (arrows, Fig. 7C,D) was also elevated compared with the same time-point at the lateral (Fig. 7E,F) and ventral (Fig. 7G,H) regions ($p=0.0003$, LMER, Tukey).

IL-$1\beta^+IBA1^+$cell density was mostly under 50 cells/mm^2 across the spinal cord regions, which was significantly reduced compared with IL-1β expressing astrocytes ($p=1.7e-35$, paired t test; compare Fig. 7 with Fig. 8). Throughout the six regions (Fig. 8C–G), the ipsilateral side to the injury showed consistently increased IL-$1\beta^+IBA1^+$ cell density compared with the contralateral side ($p=1.2e-5$, LMER). Red-light treatment had no significant effect on IL-$1\beta^+IBA1^+$ cell density ($p=0.97$, LMER).

These results demonstrate that IL-1β-expressing glial cells were present throughout the spinal cord following hemi-contusion with higher numbers on the ipsilateral side. Red-light treatment had no significant effect on IL-1β expression from either astrocytes or microglia/macrophages.

Red-light reduces iNOS-producing microglia/macrophages at the injury zone

NO is produced by iNOS in microglia/macrophages, and contributes to neuropathic pain processing.[31] Microglia/macrophages produce the iNOS isoform that can be detected by uNOS staining, which labels all three NOS isoforms (eNOS, nNOS, and iNOS). Six spinal cord regions (Fig. 9A) were triple stained for uNOS/IBA1/DAPI to investigate the density of iNOS-producing microglia/macrophages in the spinal cord following injury and red-light treatment. An example of staining is shown in Figure 9B. Throughout the six regions (Fig. 9C–H), there was significantly greater $uNOS^+/IBA1^+$ cell density on the ipsilateral side ($p=1.2e-05$, LMER), a strong effect of time ($p=0.0005$), and a significant reduction in the red-light-treated group ($p=0.0203$).

In the dorsal region of the spinal cord, $uNOS^+IBA1^+$ cells were maintained below 50 per mm^2 on the contralateral side throughout the recovery period in both groups (Fig. 9C). However, on the ipsilateral side (Fig. 9D), the 5-dpi time was significantly elevated compared with the 1- and 7-dpi times ($p=0.0010$ and 0.0075 respectively, LMER, Tukey), and a similar pattern was evident in the ipsilateral ventral region (Fig. 9H) between the 5- and 7-dpi times ($p=0.0003$, LMER, Tukey).

Although red-light significantly reduced $uNOS^+IBA1^+$ cell density overall, the effects arose mainly from the dorsal ipsilateral region across all time-points (Fig. 9D), and most strongly at the 7-dpi time.

These results show that iNOS expressing $IBA1^+$ cells are present, predominantly on the ipsilateral side following hemi-contusion SCI, and red-light treatment reduces iNOS expression, particularly at the injury focus in the ipsilateral dorsal region.

Discussion

Over the past decade, the use of photobiomodulation as a non-invasive therapy to improve repair of the injured nervous system and to reduce pain has gained increasing attention. Here, we characterized changes in mechanical sensitivity and spinal cord cellular environment in the subacute phase following a mild weight-drop hemi-contusion SCI and red-light (670 nm) treatment. We demonstrate that daily 30-min treatments of 670 nm at 35 mW/cm^2 reduces the level of mechanical sensitivity in both SCI and sham-operated rats, as well as the overall incidence of animals developing hypersensitivity following SCI. These functional improvements in SCI animals were accompanied by reduced neuronal cell death, reduced iNOS expression in $IBA1^+$microglia/macrophages, and reduced astrocyte activation but not the IL-$1\beta^+$ astrocyte subpopulation in the injured spinal cord.

The current study used an LED array with 35 W/cm^2 to treat the animals over a transparent box. This brought the light source 10 mm away from direct contract with the skin surface. Although placing the LED array closer to the animal would increase irradiance, and therefore improve penetration of the red-light, we have previously shown that 670 nm penetration is not linear to irradiance.[32] Photobiomodulation may involve both cellular or humoral factors,[33] yet the optimal and/or therapeutic window of irradiance for these differing mechanisms remains unknown. As such, dedicated studies would be required to determine the impact of removing the transparent box on animal recovery, as increasing light intensity can potentially be harmful.[34]

The treatment in the current study was carried out on animals with acute SCI. To date, complete studies examining the effects of photobiomodulation on chronic SCI remains limited; however, a clinical trial is currently recruiting participants,[35] and during the trial investigators plan to implant an irradiation fiber into the injury site to treat acute SCI. Results in chronic brain injury have been encouraging; one study has shown that 18 sessions of LED

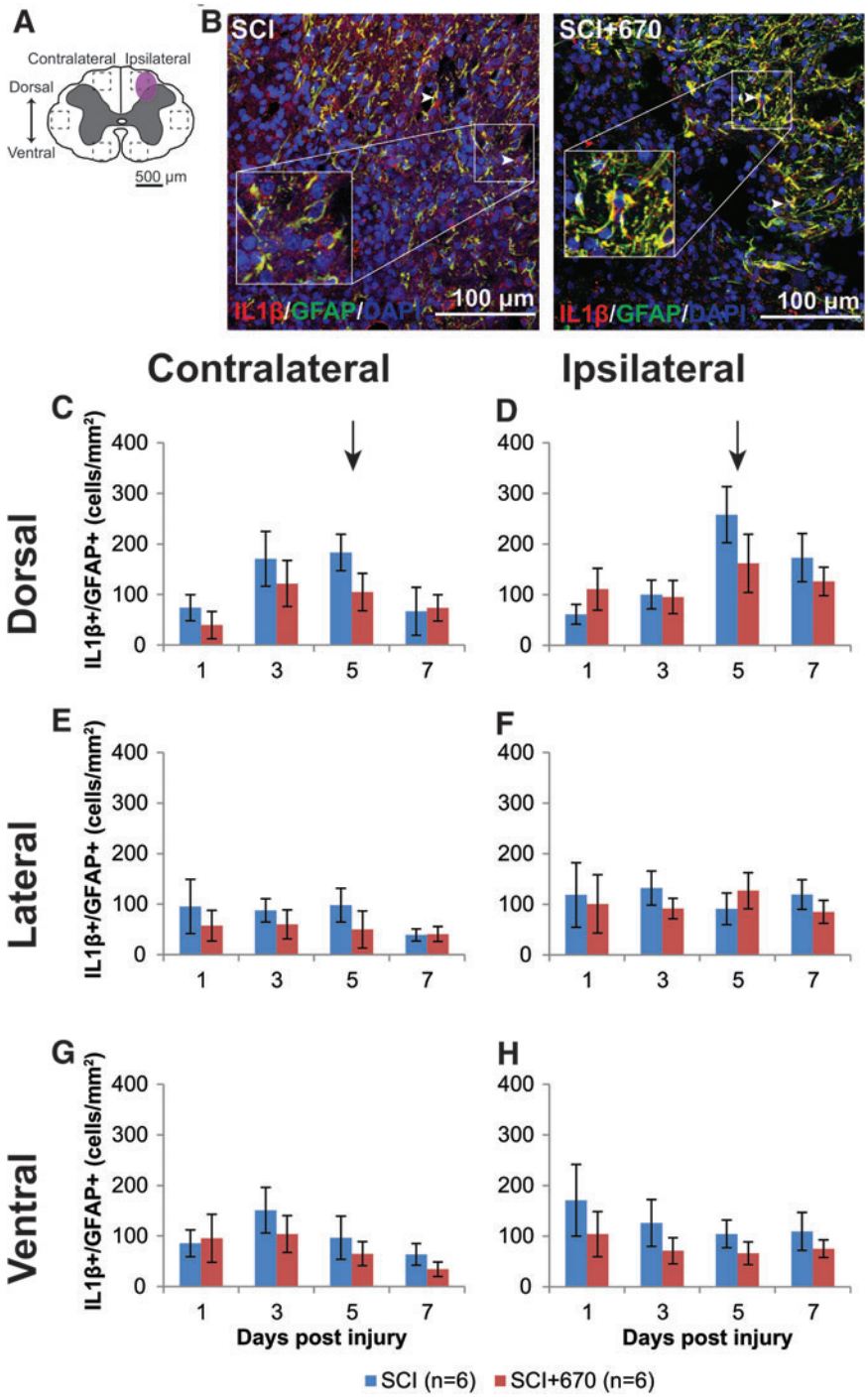

FIG. 7. The density of IL-1β producing astrocytes is not affected by red-light treatment following mild T10 hemi-contusion. **(A)** The schematic representation of the spinal cord illustrates the dorsal, lateral, and ventral regions of interest for analysis (enclosed by dashed lines, area of each box: 0.1 mm^2). Approximate location of injury is indicated by the purple shaded area. **(B)** Example images of IL-1β (red), GFAP (green), and DAPI (blue) triple-positive cells from spinal-cord injured untreated and light-treated groups ipsilateral to the injury at dorsal region at 7 dpi. **(C,D)** Quantification of IL-1β^+GFAP$^+$DAPI$^+$ cells, expressed as triple-positive cell density within the region of interest, in the dorsal region of the spinal cord, contralateral (C) and ipsilateral (D) to the spinal cord injury of untreated and light-treated groups. **(E,F)** IL-1β^+GFAP$^+$DAPI$^+$ cell density in the lateral regions of interest contralateral (E) and ipsilateral (F) to the injury. (**G,H**) IL-1β^+GFAP$^+$DAPI$^+$ cell density in the ventral regions of interest contralateral (G) and ipsilateral (H) to the injury. For each time-point n values are indicated (legend). Arrows indicate the 5-dpi time-point is significantly increased in the dorsal region compared with lateral and ventral regions ($p = 0.0003$, LMER, Tukey). Data are expressed as mean ± SEM. dpi, day post-injury; GFAP, glial fibrillary acidic protein; IL-1β, interleukin 1 beta; LMER, linear mixed-effects models; SCI, spinal-cord injured animals without red-light treatment; SCI+670, spinal-cord injured animals with red-light treatment; SEM, standard error of the mean. Color image is available online.

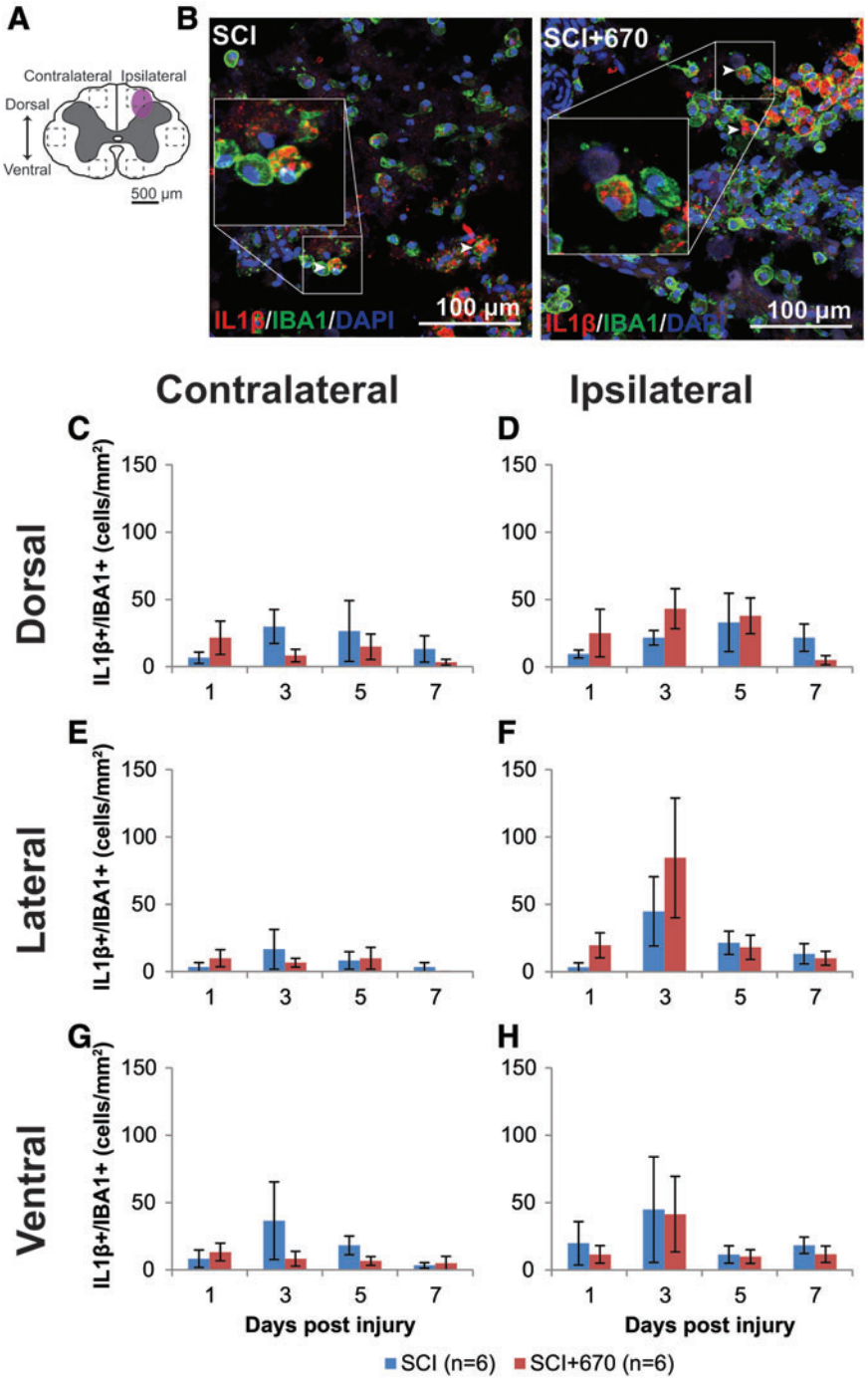

FIG. 8. IL-1β producing microglia/macrophage population is not affected by red-light treatment following T10 hemi-contusion. **(A)** The schematic representation of the spinal cord illustrates the dorsal, lateral, and ventral regions of interest for analysis (enclosed by dashed lines, area of each box: 0.1 mm^2). Approximate location of injury is indicated by the purple shaded area. **(B)** Example images shown of IL-1β (red), IBA1 (green), and DAPI (blue) triple-positive cells from spinal-cord injured untreated and light-treated groups at the dorsal level, ipsilateral to the injury at 7 dpi. **(C,D)** Quantification of IL-1β^+IBA1$^+$DAPI$^+$ cells, expressed as triple-positive cell density within the region of interest, are shown for the dorsal region of the spinal cord, contralateral (C) and ipsilateral (D) to the injury of untreated and light-treated groups. **(E,F)** IL-1β^+IBA1$^+$DAPI$^+$ cell density in the lateral regions of interest contralateral (E) and ipsilateral (F) to the injury. **(G,H)** IL-1β^+IBA1$^+$DAPI$^+$ cell density in the ventral regions of interest contralateral (G) and ipsilateral (H) to the injury. For each time-point n values are indicated (legend) . Data are expressed as mean ± SEM. dpi, day post-injury; IL-1β, interleukin 1 beta; SCI, spinal-cord injured animals without red-light treatment; SCI+670, spinal-cord injured animals with red-light treatment; SEM, standard error of the mean. Color image is available online.

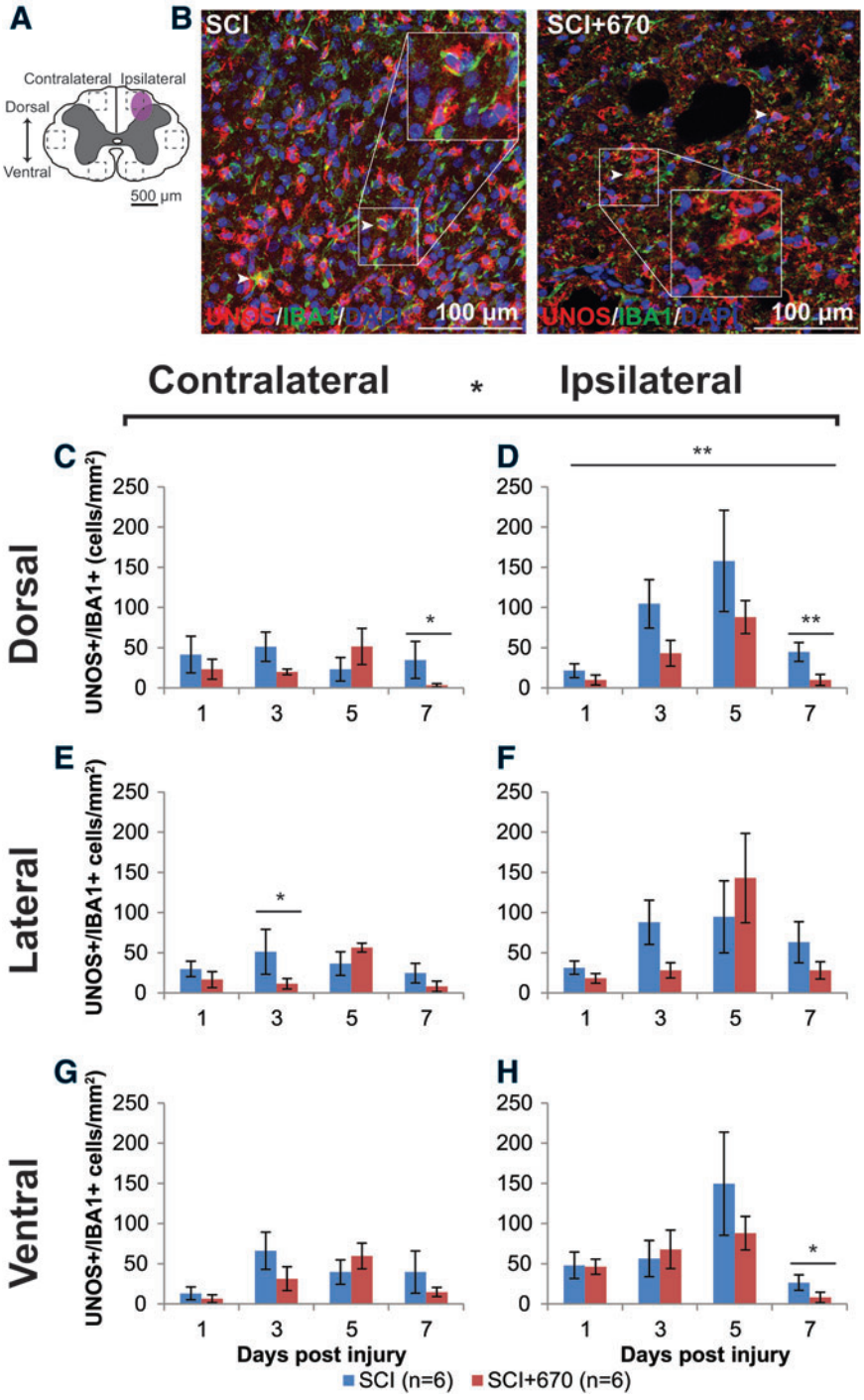

FIG. 9. iNOS expressing microglia/macrophage immunoreactivity is reduced by red-light treatment following T10 hemi-contusion. **(A)** The schematic representation of the spinal cord illustrates the dorsal, lateral, and ventral regions of interest for analysis (enclosed by dashed lines, area of each box: 0.1 mm^2). Approximate location of injury is indicated by the purple shaded area. **(B)** Example images are shown of uNOS (red), IBA1 (green), and DAPI (blue) triple-positive cells from spinal-cord injured untreated and light-treated animals at the dorsal region, ipsilateral to the injury at 7 dpi. **(C,D)** Quantification of $uNOS^+IBA1^+DAPI^+$ cells, expressed as triple-positive cell density within the dorsal region of interest, is shown contralateral (C) and ipsilateral (D) to the injury of untreated and light-treated groups. **(E,F)** $uNOS^+IBA1^+DAPI^+$ cell density in the lateral regions of interest contralateral (E) and ipsilateral (F) to the injury. **(G,H)** $uNOS^+IBA1^+DAPI^+$ cell density in the ventral regions of interest contralateral (G) and ipsilateral (H) to the injury. For each time-point *n* values are indicated (legend). Data are expressed as mean ± SEM; $*p < 0.05$, $**p < 0.01$, LMER. dpi, day post-injury; IL-1β, interleukin 1 beta; iNOS, inducible nitric oxide synthase; LMER, linear mixed-effects models; SCI, spinal-cord injured animals without red-light treatment; SCI+670, spinal-cord injured animals with red-light treatment; SEM, standard error of the mean. Color image is available online.

treatment (22.2 mW/cm^2) over 6 weeks significantly improved the cognition of patients with chronic mild traumatic brain injury.[36]

We used a mechanical testing paradigm that allowed assessment of above-, at-, and below-injury dermatomes, which provides an insight as to how mechanical sensitivity is changed following SCI. Categories 1 and 2 are not characteristic of nocifensive behaviors in laboratory rats, whereas categories 3 and 4 are inexorable behavioral responses to aversive stimuli including basic/integrated motor responses (jumping, avoidance, and aggression) and vocalization.[37] As the CON group generally displayed category 1 and 2 responses (Fig. 1A), the mechanical sensitivity used in the current study does not induce pain in normal rats. The paradigm used to assess mechanical sensitivity in the present study presents some advantages over conventional assessment methods, such as using von Frey filaments to assess paw withdrawal threshold,[20,38–40] which requires complete intact motor function of the respective limbs.[41] In addition, the display of nocifensive behavior is not affected by hindlimb(s) motor deficits; animals are capable of avoidance behaviors using the forelimbs only.

Using the predefined hypersensitivity threshold based on responses from normal intact animals, we were able to determine the percentage of animals developing hypersensitivity. This variation in the development of mechanical sensitivity is also observed in patients with SCI.[3,5,6] SCI-induced mechanical allodynia was observed in at least 50% of the rats from 1 dpi, whereas the subpopulation developing hypersensitivity was reduced by 670 nm treatment from 1 dpi to 5 dpi (Table 1). This mechanical hypersensitivity incidence in untreated SCI animals is consistent with another study that reported 67%,[42] and with our previous study of hypersensitivity incidence at 7 dpi using a more severe SCI model.[21] The current study provides the first evidence that 670 nm treatment reduces hypersensitivity incidence in the subacute phase following SCI in rats.

There could be two possible explanations for the early reduction in hypersensitivity incidence; 670 nm light could either delay the development, or accelerate the recovery, of mechanical hypersensitivity. The latter is likely because 670 nm treatment has been shown to accelerate cellular processes and increase metabolism.[43–45] Further, the peak hypersensitivity in the light-treated group was at 5 dpi (Supplementary Fig. S2), whereas the untreated injured group appeared to continue to develop hypersensitivity over the 7-day recovery period, and therefore, might require more time to fully develop maximal hypersensitivity.

As expected, only a few sham-injured animals were categorized as hypersensitive, suggesting that the surgical procedure does not produce excessive pain in the dorsum of the animal. Hypersensitive untreated animals with SCI develop mechanical hypersensitivity mostly in the At-Level regions from 1 dpi with the potential to develop Below-Level hypersensitivity by 7 dpi. These results are consistent with patients with SCI in clinical settings. Neuropathic pain patients develop both early-onset At-Level and late-onset Below-Level allodynia/hyperalgesia.[5,7,8,31,46,47] Although changes at the spinal and the supraspinal level have been correlated with the development of these two distinct pain phenotypes, the exact underlying mechanism remains unclear.[5,48–50] As we previously showed that the reduction in mechanical sensitivity is not due to reduced functional integrity of the dorsal column pathway,[21] it may arises from the anterolateral system. Following the surgery, bradykinins are released that elicit pain/sensitization in the skin, whereas endogenous opioids such as endorphins are produced to control the pain.[51] Photobiomodulation has been shown to decrease bradykinins while increasing endorphins,[52,53] therefore the effect of red-light in the present study may result from alterations to bradykinins and/or endogenous opioids, leading to an overall reduction in sensitivity across all groups.

Little is known about the effect of red-light treatment on myelination. In the current study, no effect of 670 nm was observed on the level of myelination. The percentage area stained with MBP was found to be around 56%, which is consistent with a previous study.[54] We and others show that demyelination starts within 24 h post-SCI.[55,56] Remyelination following SCI starts around 7 dpi,[56] which is consistent with our MBP levels similar to CONs at 7 dpi (Fig. 3). Up to date, there have been no studies documenting the effect of 670 nm treatment on demyelination following SCI. The most relevant study using 650 nm following sciatic nerve injury found no effect on the number of Schwann cells in rabbits at 30 dpi.[57] It has been shown that demyelination also occurs in rostral and caudal regions.[58] Further investigations are thus needed to examine the effect of 670 nm on myelination outside the injury epicenter.

Studies have shown rapid loss of NF200 (especially dephosphorylated population) following SCI within the first 24 h,[59] which was consistent with our findings (Fig. 4). Disrupted and degraded neurofilament then leads to axonal degeneration,[60,61] which could contribute to pain hypersensitivity. A 670 nm treatment was not effective in stalling the loss of NF200. A similar result was found in a model of sciatic nerve injury in rabbits, where no effect of 650 nm was found on the number of myelinated axons at 30 dpi.[57] It is therefore worth investigating changes in axons rostral and caudal to the injury, as loss of neurofilament is well documented in those areas following SCI.[58]

Neuronal cells undergo apoptosis and necrosis following SCI, whereas there is minimal neuronal death in naïve spinal cords.[62–64] Most neuronal death was observed in the dorsal and intermediate levels, which would give rise to neurons in the spinothalamic tract, visceral motor neurons, and interneurons. It is therefore not feasible to speculate which type(s) is more susceptible to cell death. A 670 nm treatment has been shown to significantly reduce neuronal cell death following SCI from 1 dpi. A similar study using 810 nm treatment showed 50% less motor neuron death following ischemia-induced SCI at 3 dpi.[65] The mechanism by which 670 nm treatment reduces neuronal cell death might be related to reduced iNOS (Fig. 9). Xu and colleagues have shown that iNOS induces spinal neuronal degeneration following SCI through extracellular signal regulated kinases.[66]

Following SCI, pro-inflammatory cytokines are secreted by activated glial cells, both microglia/macrophages and astrocytes. During the post-injury period, these glial cells are activated through a combination of different mechanisms that involve neuroinflammation, ionic imbalance, and cytokines/chemokines.[46] Regional and global increases in GFAP expression have been documented from 2 h persisting for at least 6 months,[46] in agreement with our observation of increased GFAP expression throughout the cord segment within 24 h post-injury, which persisted for at least 7 days (Fig. 6). Limited studies have shown the effect of 670 nm treatment following SCI on astrocyte activation or GFAP upregulation, although similar effects using 810 nm have been documented.[22] Other groups have previously demonstrated a reduction in GFAP expression following light treatment in Müller cells in the retina,[67,68] and a decrease in GFAP expression by 670 nm irradiation in the brain of monkeys with Parkinson's disease.[69]

The present study is the first demonstration that GFAP upregulation in astrocytes is reduced by daily 670 nm treatment from 3 dpi

following SCI. The reduced GFAP cannot account for the early (i.e., 1 dpi) red-light-induced pain relief, as GFAP expression was not reduced at this time. Surprisingly, the reduction in GFAP did not appear to arise from the IL-1β astrocyte subpopulation (Fig. 7). IL-1β is strongly implicated in the development of pain hypersensitivity.[70] Subpopulations of GFAP$^+$ astrocytes have been reported before and IL-1β^+ astrocytes are considered to be pro-inflammatory and neurotoxic.[71] However, it is possible that red-light modulates other mediators or astrocyte subpopulations.

IL-1β, produced by both astrocytes and microglia/macrophages, is a cytokine that not only augments inflammation, but also acts on both pre- and post-synaptic terminals to initiate and maintain pain.[70,72] We found no effect of 670 nm treatment on IL-1β production in microglia/macrophages following SCI from 1 to 7 dpi (Fig. 8). This observation is consistent with our previous study[21] showing no effect of 670 nm on pro-inflammatory microglia/macrophage (M1), and another study where the authors showed no effect of 810 nm on IL-1β expression at either 6 h post-injury or 4 dpi following SCI.[22] However, other studies have reported decreases in IL-1β expression by light treatment in other injury models.[73,74] This discrepancy suggests that light treatment may activate different cell pathways in different injury models. As IL-1β is a significant player in the regulation of pain, the present study suggests that the pain-alleviating effect of 670 nm light treatment may be independent, or downstream from IL-1β, at least up to the first 7 days. Further, we found a reduction in the behavioral sensitivity of red-light treated sham-injured animals (Fig. 1C). The mechanism of the red-light-induced reduction of sensitivity in these animals is also unlikely to be IL-1β-dependant because these animals displayed no evidence of pain behaviors.

We also found a significant decrease in uNOS expression, a surrogate marker for iNOS in microglia/macrophages, following 670 nm treatment in animals with SCI (Fig. 9). Byrnes and associates found a significant reduction in iNOS transcription that was measured by real-time polymerase chain reaction (RT-PCR) at 6 h post-injury, but not at 4 dpi using 810 nm treatment.[22] The discrepancy between our study and that of Byrnes and associates at 3–4 dpi might indicate a different mechanism of action between 670 nm and 810 nm, or that the reduction of iNOS$^+$ microglia/macrophages was masked by an increase of iNOS in other cells types not observed by the investigators. It is interesting that IL-1β and iNOS, both considered markers of classically activated microglia/macrophages (M1), were affected differently by red-light treatment.

In our previous study, we demonstrated that red-light did not alter the proportion of M1 cells; however, the proportion of M2 cells was increased.[21] The current study is partly consistent with this idea; IL-1β-expressing cells (M1 phenotype) were not altered by red-light treatment; however, immunoreactive iNOS (another marker of M1 phenotype) microglia/macrophages were reduced. iNOS downregulation may indirectly indicate conversion toward arginase upregulation[75] and therefore conversion toward the M2 phenotype. It may be possible that iNOS and IL-1β are produced by different cells and that the decrease in iNOS expression in microglia/macrophages might occur in response to the increase in M2 microglia/macrophage.[21] In addition to the beneficial effect of a less inflammatory microenvironment, the decreased iNOS expression in microglia/macrophages could also contribute to the reduced mechanical sensitivity in 670 nm treated animals. Studies have shown that pain following SCI could be reduced, or reversed, by iNOS inhibitors or general NOS inhibition.[76,77] The present study supports the idea that 670 nm may act on a pain modulation pathway that is iNOS-dependent, but IL-1β-independent. Future studies examining these ideas would be of interest. Moreover, future studies using stereology, such as the optical fractionator technique,[78] to quantify 670 nm-induced changes in neuron and glial cell numbers in the entire spinal cord structure would be of interest.

In conclusion, we demonstrate that daily 670 nm irradiation reduces mechanical sensitivity in SCI and in sham-operated rats, and reduces the chance of developing hypersensitivity up to 5 days post-SCI. The analgesic effects of red-light therapy in the subacute stage after SCI may involve reduced neuronal death, reduced astrogliosis, and reduced iNOS expression in microglia/macrophage in the spinal cord, independent of myelination and IL-1β glial cell expression. The combined reduction of iNOS$^+$ microglia/macrophages and IL-1β^- astrocytes may therefore impact different stages of mechanical sensitivity following SCI. Taken together, these findings suggest that red-light therapy can be a safe non-pharmacological approach to manage pain by modulating the endogenous response of neuronal and glial populations following SCI.

Funding Information

The authors gratefully acknowledge the Bootes Medical Research Foundation for funding this project.

Author Disclosure Statement

No competing financial interests exist.

Supplementary Material

Supplementary Figure S1
Supplementary Figure S2
Supplementary Figure S3
Supplementary Figure S4

References

1. World Health Organization and International Spinal Cord Society. (2013). International perspectives on spinal cord injury. World Health Organization: Geneva, Switzerland. https://apps.who.int/iris/bitstream/handle/10665/94190/9789241564663_eng.pdf;jsessionid=DE35C51564EE4EF78261AF364CC5282E?sequence=1
2. Singh, A., Tetreault, L., Kalsi-Ryan, S., Nouri, A., and Fehlings, M.G. (2014). Global prevalence and incidence of traumatic spinal cord injury. Clin. Epidemiol. 6, 309–331.
3. Turner, J.A., Cardenas, D.D., Warms, C.A., and McClellan, C.B. (2001). Chronic pain associated with spinal cord injuries: a community survey. Arch. Phys. Med. Rehabil. 82, 501–509.
4. Pascoal-Faria, P., Yalcin, N., and Fregni, F. (2015). Neural markers of neuropathic pain associated with maladaptive plasticity in spinal cord injury. Pain Pract. 15, 371–377.
5. Finnerup, N.B., Norrbrink, C., Trok, K., Piehl, F., Johannesen, I.L., Sorensen, J.C., Jensen, T.S., and Werhagen, L. (2014). Phenotypes and predictors of pain following traumatic spinal cord injury: a prospective study. J. Pain 15, 40–48.
6. Dijkers, M., Bryce, T., and Zanca, J. (2009). Prevalence of chronic pain after traumatic spinal cord injury: a systematic review. J. Rehabil. Res. Dev. 46, 13–29.
7. Bryce, T.N. (2009). *Spinal Cord Injury*. Springer Publishing Company.
8. Widerstrom-Noga, E., Biering-Sorensen, F., Bryce, T.N., Cardenas, D.D., Finnerup, N.B., Jensen, M.P., Richards, J.S., and Siddall, P.J. (2014). The International Spinal Cord Injury Pain Basic Data Set (version 2.0). Spinal Cord 52, 282–286.
9. Finnerup, N.B., Johannesen, I.L., Fuglsang-Frederiksen, A., Bach, F.W., and Jensen, T.S. (2003). Sensory function in spinal cord injury patients with and without central pain. Brain 126, 57–70.
10. D'Angelo, R., Morreale, A., Donadio, V., Boriani, S., Maraldi, N., Plazzi, G., and Liguori, R. (2013). Neuropathic pain following spinal cord injury: what we know about mechanisms, assessment and management. Eur. Rev. Med. Pharmacol. Sci. 17, 3257–3261.

11. Chiang, C.Y., Sessle, B.J., and Dostrovsky, J.O. (2012). Role of astrocytes in pain. Neurochem. Res. 37, 2419–2431.
12. Nakajima, A., Tsuboi, Y., Suzuki, I., Honda, K., Shinoda, M., Kondo, M., Matsuura, S., Shibuta, K., Yasuda, M., Shimizu, N., and Iwata, K. (2011). PKCgamma in Vc and C1/C2 is involved in trigeminal neuropathic pain. J. Dent. Res. 90, 777–781.
13. Kobayashi, A., Shinoda, M., Sessle, B.J., Honda, K., Imamura, Y., Hitomi, S., Tsuboi, Y., Okada-Ogawa, A., and Iwata, K. (2011). Mechanisms involved in extraterritorial facial pain following cervical spinal nerve injury in rats. Mol. Pain 7, 12.
14. Ji, R.R., Gereau, R.W., 4th, Malcangio, M., and Strichartz, G.R. (2009). MAP kinase and pain. Brain Res. Rev. 60, 135–148.
15. Nakagawa, T., and Kaneko, S. (2010). Spinal astrocytes as therapeutic targets for pathological pain. J. Pharmacol. Sci. 114, 347–353.
16. McMahon, S.B., and Malcangio, M. (2009). Current challenges in glia-pain biology. Neuron 64, 46–54.
17. Ikeda, H., Stark, J., Fischer, H., Wagner, M., Drdla, R., Jager, T., and Sandkuhler, J. (2006). Synaptic amplifier of inflammatory pain in the spinal dorsal horn. Science 312, 1659–1662.
18. Galan-Arriero, I., Avila-Martin, G., Ferrer-Donato, A., Gomez-Soriano, J., Bravo-Esteban, E., and Taylor, J. (2014). Oral administration of the p38alpha MAPK inhibitor, UR13870, inhibits affective pain behavior after spinal cord injury. Pain 155, 2188–2198.
19. Watanabe, S., Uchida, K., Nakajima, H., Matsuo, H., Sugita, D., Yoshida, A., Honjoh, K., Johnson, W.E., and Baba, H. (2015). Early transplantation of mesenchymal stem cells after spinal cord injury relieves pain hypersensitivity through suppression of pain-related signaling cascades and reduced inflammatory cell recruitment. Stem Cells 33, 1902–1914.
20. Tateda, S., Kanno, H., Ozawa, H., Sekiguchi, A., Yahata, K., Yamaya, S., and Itoi, E. (2017). Rapamycin suppresses microglial activation and reduces the development of neuropathic pain after spinal cord injury. J. Orthop. Res. 35, 93–103.
21. Hu, D., Zhu, S., and Potas, J.R. (2016). Red LED photobiomodulation reduces pain hypersensitivity and improves sensorimotor function following mild T10 hemicontusion spinal cord injury. J. Neuroinflammation 13, 200.
22. Byrnes, K.R., Waynant, R.W., Ilev, I.K., Wu, X., Barna, L., Smith, K., Heckert, R., Gerst, H., and Anders, J.J. (2005). Light promotes regeneration and functional recovery and alters the immune response after spinal cord injury. Lasers Surg. Med. 36, 171–185.
23. Yang, X., Askarova, S., Sheng, W., Chen, J.K., Sun, A.Y., Sun, G.Y., Yao, G., and Lee, J.C. (2010). Low energy laser light (632.8 nm) suppresses amyloid-beta peptide-induced oxidative and inflammatory responses in astrocytes. Neuroscience 171, 859–868.
24. Vijayaprakash, K.M., and Sridharan, N. (2013). An experimental spinal cord injury rat model using customized impact device: a cost-effective approach. J. Pharmacol. Pharmacother. 4, 211–213.
25. Schneider, C.A., Rasband, W.S., and Eliceiri, K.W. (2012). NIH Image to ImageJ: 25 years of image analysis. Nat. Methods 9, 671–675.
26. R Core Team. (2016). *R: A Language and Environment for Statistical Computing*. R Foundation for Statistical Computing: Vienna, Austria.
27. Kuznetsova, A., Brockhoff, P.B., and Christensen, R.H.B. (2017). lmerTest: Tests in Linear Mixed Effects Models. J. Statist. Soft. 82, 1–26.
28. McElreath, R. (2015). Overfitting, regularization, and information criteria, in: *Statistical Rethinking: A Bayesian Course with Examples in R and Stan*, 1st edition. R. McElreath (ed). CRC Press: Boca Raton, FL, pps. 165–207.
29. Christensen R.H.B. (2019). ''ordinal—Regression Models for Ordinal Data.'' R package version 2019.12-10. https://CRAN.R-project.org/package=ordinal
30. Ji, R.R., Berta, T., and Nedergaard, M. (2013). Glia and pain: is chronic pain a gliopathy? Pain 154, Suppl. 1, S10–S28.
31. Hulsebosch, C.E., Hains, B.C., Crown, E.D., and Carlton, S.M. (2009). Mechanisms of chronic central neuropathic pain after spinal cord injury. Brain Res. Rev. 60, 202–213.
32. Hu, D., van Zeyl, M., Valter, K., and Potas, J.R. (2019). Sex, but not skin tone affects penetration of red-light (660 nm) through sites susceptible to sports injury in lean live and cadaveric tissues. J. Biophotonics, e201900010.
33. Johnstone, D.M., Moro, C., Stone, J., Benabid, A.L., and Mitrofanis, J. (2015). Turning on lights to stop neurodegeneration: the potential of near infrared light therapy in Alzheimer's and Parkinson's disease. Front. Neurosci. 9, 500.
34. Chu-Tan, J.A., Rutar, M., Saxena, K., Wu, Y., Howitt, L., Valter, K., Provis, J., and Natoli, R. (2016). Efficacy of 670 nm light therapy to protect against photoreceptor cell death is dependent on the severity of damage. Int. J. Photoenergy 2016, 1–12.
35. Xijing Hospital. (2018). Clinical study of treatment of acute spinal cord injury by near infrared light irradiation. ClincalTrials.gov, U.S. National Library of Medicine. https://ClinicalTrials.gov/show/NCT03643419
36. Naeser, M.A., Zafonte, R., Krengel, M.H., Martin, P.I., Frazier, J., Hamblin, M.R., Knight, J.A., Meehan, W.P., 3rd, and Baker, E.H. (2014). Significant improvements in cognitive performance post-transcranial, red/near-infrared light-emitting diode treatments in chronic, mild traumatic brain injury: open-protocol study. J. Neurotrauma 31, 1008–1017.
37. Institute for Laboratory Animal Research (U.S.). Committee on Recognition and Alleviation of Pain in Laboratory Animals. (2009). *Recognition and Alleviation of Pain in Laboratory Animals*. National Academies Press: Washington, D.C.
38. Kanno, H., Pressman, Y., Moody, A., Berg, R., Muir, E.M., Rogers, J.H., Ozawa, H., Itoi, E., Pearse, D.D., and Bunge, M.B. (2014). Combination of engineered Schwann cell grafts to secrete neurotrophin and chondroitinase promotes axonal regeneration and locomotion after spinal cord injury. J. Neurosci 34, 1838–1855.
39. Bartus, K., James, N.D., Didangelos, A., Bosch, K.D., Verhaagen, J., Yanez-Munoz, R.J., Rogers, J.H., Schneider, B.L., Muir, E.M., and Bradbury, E.J. (2014). Large-scale chondroitin sulfate proteoglycan digestion with chondroitinase gene therapy leads to reduced pathology and modulates macrophage phenotype following spinal cord contusion injury. J. Neurosci. 34, 4822–4836.
40. Yu, D., Thakor, D.K., Han, I., Ropper, A.E., Haragopal, H., Sidman, R.L., Zafonte, R., Schachter, S.C., and Teng, Y.D. (2013). Alleviation of chronic pain following rat spinal cord compression injury with multimodal actions of huperzine A. Proc. Natl. Acad. Sci. U S A 110, E746–E755.
41. Detloff, M.R., Clark, L.M., Hutchinson, K.J., Kloos, A.D., Fisher, L.C., and Basso, D.M. (2010). Validity of acute and chronic tactile sensory testing after spinal cord injury in rats. Exp. Neurol. 225, 366–376.
42. Siddall, P., Xu, C.L., and Cousins, M. (1995). Allodynia following traumatic spinal cord injury in the rat. Neuroreport 6, 1241–1244.
43. Begum, R., Calaza, K., Kam, J.H., Salt, T.E., Hogg, C., and Jeffery, G. (2015). Near-infrared light increases ATP, extends lifespan and improves mobility in aged Drosophila melanogaster. Biol. Lett. 11, 20150073.
44. Yip, K.K., Lo, S.C., Leung, M.C., So, K.F., Tang, C.Y., and Poon, D.M. (2011). The effect of low-energy laser irradiation on apoptotic factors following experimentally induced transient cerebral ischemia. Neuroscience 190, 301–306.
45. Eells, J.T., Henry, M.M., Summerfelt, P., Wong-Riley, M.T., Buchmann, E.V., Kane, M., Whelan, N.T., and Whelan, H.T. (2003). Therapeutic photobiomodulation for methanol-induced retinal toxicity. Proc. Natl. Acad. Sci. U S A100, 3439–3444.
46. Gwak, Y.S., Kang, J., Unabia, G.C., and Hulsebosch, C.E. (2012). Spatial and temporal activation of spinal glial cells: role of gliopathy in central neuropathic pain following spinal cord injury in rats. Exp. Neurol. 234, 362–372.
47. Finnerup, N.B., Baastrup, C., and Jensen, T.S. (2009). Neuropathic pain following spinal cord injury pain: mechanisms and treatment. Scand. J. Pain 1, S3–S11.
48. Siddall, P.J., McClelland, J.M., Rutkowski, S.B., and Cousins, M.J. (2003). A longitudinal study of the prevalence and characteristics of pain in the first 5 years following spinal cord injury. Pain 103, 249–257.
49. Wrigley, P.J., Press, S.R., Gustin, S.M., Macefield, V.G., Gandevia, S.C., Cousins, M.J., Middleton, J.W., Henderson, L.A., and Siddall, P.J. (2009). Neuropathic pain and primary somatosensory cortex reorganization following spinal cord injury. Pain 141, 52–59.
50. Hari, A.R., Wydenkeller, S., Dokladal, P., and Halder, P. (2009). Enhanced recovery of human spinothalamic function is associated with central neuropathic pain after SCI. Exp. Neurol. 216, 428–430.
51. Stein, C., Clark, J.D., Oh, U., Vasko, M.R., Wilcox, G.L., Overland, A.C., Vanderah, T.W., and Spencer, R.H. (2009). Peripheral mechanisms of pain and analgesia. Brain Res. Rev. 60, 90–113.
52. Lins, R.D., Dantas, E.M., Lucena, K.C., Catao, M.H., Granville-Garcia, A.F., and Carvalho Neto, L.G. (2010). Biostimulation effects of low-power laser in the repair process. An. Bras. Dermatol. 85, 849–855.

53. Chaves, M.E., Araujo, A.R., Piancastelli, A.C., and Pinotti, M. (2014). Effects of low-power light therapy on wound healing: LASER x LED. An. Bras. Dermatol. 89, 616–623.
54. Crocker, S.J., Whitmire, J.K., Frausto, R.F., Chertboonmuang, P., Soloway, P.D., Whitton, J.L., and Campbell, I.L. (2006). Persistent macrophage/microglial activation and myelin disruption after experimental autoimmune encephalomyelitis in tissue inhibitor of metalloproteinase-1-deficient mice. Am. J. Pathol. 169, 2104–2116.
55. Lasiene, J., Shupe, L., Perlmutter, S., and Horner, P. (2008). No evidence for chronic demyelination in spared axons after spinal cord injury in a mouse. J. Neurosci. 28, 3887–3896.
56. Totoiu, M.O., and Keirstead, H.S. (2005). Spinal cord injury is accompanied by chronic progressive demyelination. J. Comp. Neurol. 486, 373–383.
57. Takhtfooladi, M.A., and Sharifi, D. (2015). A comparative study of red and blue light-emitting diodes and low-level laser in regeneration of the transected sciatic nerve after an end to end neurorrhaphy in rabbits. Lasers Med. Sci. 30, 2319–2324.
58. Kozlowski, P., Raj, D., Liu, J., Lam, C., Yung, A.C., and Tetzlaff, W. (2008). Characterizing white matter damage in rat spinal cord with quantitative MRI and histology. J. Neurotrauma 25, 653–676.
59. Schumacher, P.A., Eubanks, J.H., and Fehlings, M.G. (1999). Increased calpain I-mediated proteolysis, and preferential loss of dephosphorylated NF200, following traumatic spinal cord injury. Neuroscience 91, 733–744.
60. Park, E., Velumian, A.A., and Fehlings, M.G. (2004). The role of excitotoxicity in secondary mechanisms of spinal cord injury: a review with an emphasis on the implications for white matter degeneration. J. Neurotrauma 21, 754–774.
61. Eftekharpour, E., Karimi-Abdolrezaee, S., and Fehlings, M.G. (2008). Current status of experimental cell replacement approaches to spinal cord injury. Neurosurg. Focus 24, E19.
62. Rosado, I.R., Lavor, M.S., Alves, E.G., Fukushima, F.B., Oliveira, K.M., Silva, C.M., Caldeira, F.M., Costa, P.M., and Melo, E.G. (2014). Effects of methylprednisolone, dantrolene, and their combination on experimental spinal cord injury. Int. J. Clin. Exp. Pathol. 7, 4617–4626.
63. Li, H.T., Zhao, X.Z., Zhang, X.R., Li, G., Jia, Z.Q., Sun, P., Wang, J.Q., Fan, Z.K., and Lv, G. (2016). Exendin-4 enhances motor function recovery via promotion of autophagy and inhibition of neuronal apoptosis after spinal cord injury in rats. Mol. Neurobiol. 53, 4073–4082.
64. Zhang, Z., Huang, Z., Dai, H., Wei, L., Sun, S., and Gao, F. (2015). Therapeutic efficacy of E-64-d, a selective calpain inhibitor, in experimental acute spinal cord injury. Biomed. Res. Int. 2015, 134242.
65. Sotoudeh, A., Jahanshahi, A., Zareiy, S., Darvishi, M., Roodbari, N., and Bazzazan, A. (2015). The influence of low-level laser irradiation on spinal cord injuries following ischemia-reperfusion in rats. Acta. Cir. Bras. 30, 611–616.
66. Xu, Z., Wang, B.R., Wang, X., Kuang, F., Duan, X.L., Jiao, X.Y., and Ju, G. (2006). ERK1/2 and p38 mitogen-activated protein kinase mediate iNOS-induced spinal neuron degeneration after acute traumatic spinal cord injury. Life Sci. 79, 1895–1905.
67. Begum, R., Powner, M.B., Hudson, N., Hogg, C., and Jeffery, G. (2013). Treatment with 670 nm light up regulates cytochrome C oxidase expression and reduces inflammation in an age-related macular degeneration model. PLoS One 8, e57828.
68. Marco, F.D., Romeo, S., Nandasena, C., Purushothuman, S., Adams, C., Bisti, S., and Stone, J. (2013). The time course of action of two neuroprotectants, dietary saffron and photobiomodulation, assessed in the rat retina. Am. J. Neurodegener. Dis. 2, 208–220.
69. El Massri, N., Moro, C., Torres, N., Darlot, F., Agay, D., Chabrol, C., Johnstone, D.M., Stone, J., Benabid, A.L., and Mitrofanis, J. (2016). Near-infrared light treatment reduces astrogliosis in MPTP-treated monkeys. Exp. Brain Res. 234, 3225–3232.
70. Calvo, M., Dawes, J.M., and Bennett, D.L. (2012). The role of the immune system in the generation of neuropathic pain. Lancet Neurol. 11, 629–642.
71. Liddelow, S.A., Guttenplan, K.A., Clarke, L.E., Bennett, F.C., Bohlen, C.J., Schirmer, L., Bennett, M.L., Munch, A.E., Chung, W.S., Peterson, T.C., Wilton, D.K., Frouin, A., Napier, B.A., Panicker, N., Kumar, M., Buckwalter, M.S., Rowitch, D.H., Dawson, V.L., Dawson, T.M., Stevens, B., and Barres, B.A. (2017). Neurotoxic reactive astrocytes are induced by activated microglia. Nature 541, 481–487.
72. Clark, A.K., Gruber-Schoffnegger, D., Drdla-Schutting, R., Gerhold, K.J., Malcangio, M., and Sandkuhler, J. (2015). Selective activation of microglia facilitates synaptic strength. The J. Neurosci. 35, 4552–4570.
73. Sahu, K., Sharma, M., and Gupta, P.K. (2015). Modulation of inflammatory response of wounds by antimicrobial photodynamic therapy. Laser Ther. 24, 201–208.
74. Lee, W.J., Lee, K.C., Kim, M.J., Jang, Y.H., Lee, S.J., and Kim, D.W. (2016). Efficacy of red or infrared light-emitting diodes in a mouse model of propionibacterium acnes-induced inflammation. Ann. Dermatol. 28, 186–191.
75. Lee, J., Ryu, H., Ferrante, R.J., Morris, S.M., Jr., and Ratan, R.R. (2003). Translational control of inducible nitric oxide synthase expression by arginine can explain the arginine paradox. Proc. Natl. Acad. Sci. U S A 100, 4843–4848.
76. Yu, Y., Matsuyama, Y., Nakashima, S., Yanase, M., Kiuchi, K., and Ishiguro, N. (2004). Effects of MPSS and a potent iNOS inhibitor on traumatic spinal cord injury. Neuroreport 15, 2103–2107.
77. Fairbanks, C.A., Schreiber, K.L., Brewer, K.L., Yu, C.G., Stone, L.S., Kitto, K.F., Nguyen, H.O., Grocholski, B.M., Shoeman, D.W., Kehl, L.J., Regunathan, S., Reis, D.J., Yezierski, R.P., and Wilcox, G.L. (2000). Agmatine reverses pain induced by inflammation, neuropathy, and spinal cord injury. Proc. Natl. Acad. Sci. U S A 97, 10584–10589.
78. Olesen, M.V., Needham, E.K., and Pakkenberg, B. (2017). The Optical fractionator technique to estimate cell numbers in a rat model of electroconvulsive therapy. J. Vis. Exp. doi: 10.3791/55737.

Address correspondence to:
Jason R. Potas, PhD
School of Medical Sciences
Wallace Wurth Building (C27)
University of New South Wales (UNSW Sydney)
Sydney, New South Wales 2052
Australia

E-mail: j.potas@unsw.edu.au